HHS Public Access

Author manuscript

Biochemistry. Author manuscript; available in PMC 2023 October 12.

Published in final edited form as:

Biochemistry. 2018 June 05; 57(22): 3176–3190. doi:10.1021/acs.biochem.7b01250.

Catalytic Mechanism of Cruzain from *Trypanosoma cruzi* As Determined from Solvent Kinetic Isotope Effects of Steady-State and Pre-Steady-State Kinetics

Xiang Zhai[†],

Thomas D. Meek[*]

Department of Biochemistry and Biophysics, Texas A&M University, College Station, Texas 77843, United States

Abstract

Cruzain, an important drug target for Chagas disease, is a member of clan CA of the cysteine proteases. Understanding the catalytic mechanism of cruzain is vital to the design of new inhibitors. To this end, we have determined pH−rate profiles for substrates and affinity agents and solvent kinetic isotope effects in presteady-state and steady-state modes using three substrates: Cbz-Phe-Arg-AMC, Cbz-Arg-Arg-AMC, and Cbz-Arg-Ala-AMC. The pH−rate profile of k_{cat}/K_m for Cbz-Arg-Arg-AMC indicated $pK_1 = 6.6$ (unprotonated) and pK_2~9.6 (protonated) groups were required for catalysis. The temperature dependence of the $pK = 6.2 - 6.6$ group exhibited a ΔH_{ion} value of 8.4 kcal/mol, typical of histidine. The pH−rate profile of inactivation by iodoacetamide confirmed that the catalytic cysteine possesses a pK_a of 9.8. Normal solvent kinetic isotope effects were observed for both $^{D_2O}k_{cat}(1.6 - 2.1)$ and $^{D_2O}k_{cat}/K_m(1.1 - 1.4)$ for all three substrates. Pre-steady-state kinetics revealed exponential bursts of AMC production for Cbz-Phe-Arg-AMC and Cbz-Arg-Arg-AMC, but not for Cbz-Arg-Ala-AMC. The overall solvent isotope effect on k_{cat} can be attributed to the solvent isotope effect on the deacylation step. Our results suggest that cruzain is unique among papain-like cysteine proteases in that the catalytic cysteine and histidine have neutral charges in the free enzyme. The generation of the active thiolate of the catalytic cysteine is likely preceded (and possibly triggered) by a ligand-induced conformational change, which could bring the catalytic dyad into the proximity to effect proton transfer.

Graphical Abstract

[*]**Corresponding Author:** tdmeek@email.tamu.edu.

[†]**Present Address:** X.Z.: Discovery Sciences, IMED Biotech Unit, AstraZeneca, R&D Boston, 35 Gatehouse Dr., Waltham, MA 02451.

Supporting Information

The Supporting Information is available free of charge on the ACS Publications website at DOI: 10.1021/acs.biochem.7b01250.

Steady-state kinetic data for wild-type cruzain-catalyzed reactions of Z-FR-AMC, Z-RR-AMC, and Z-RA-AMC in H_2O and D_2O and E208A mutant cruzain-catalyzed reactions of Z-FR-AMC, Z-RR-AMC, and Z-RA-AMC in H_2O; pK values of E208A cruzain; pH−rate profiles of the E208A mutant-catalyzed reactions of Z-FR-AMC, Z-RR-AMC, and Z-RA-AMC in H_2O; and pre-steady-state data and replots of pre-steady-state kinetic constants for the wild-type cruzain-catalyzed reaction of Z-RR-AMC in H_2O and D_2O (PDF)

The authors declare no competing financial interest.

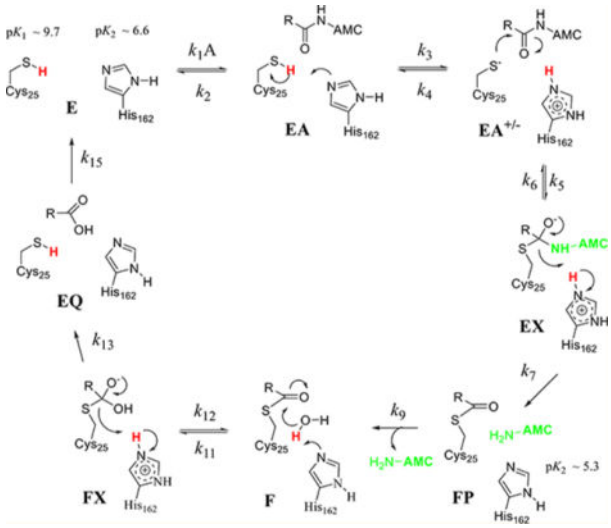

Cruzain is the major cysteine protease expressed by *Trypanosoma cruzi*, the causative agent of Chagas disease.[1] With Chagas disease categorized as one of the most important neglected tropical diseases (NTDs), it is estimated that almost 8–9 million people are currently affected by this disease, with 50000 new cases annually reported in Latin America and the Caribbean.[2] Present treatment options of Chagas disease are limited to benznidazole and nifurtimox, both of which have severe side effects and are inefficacious against long-term infections.[3] The viability of cruzain as a drug target for new trypanocidal agents was demonstrated both in cell culture[4,5] and in animal models,[6,7] although its exact physiological role remains unclear. Recent studies have suggested that cruzain is potentially involved in immune evasion through its proteolysis of NF-κB P65,[8] and the activation of latent TGF-β that induces increased infectivity of *T. cruzi*.[9]

Extensive efforts over the past three decades to develop inhibitors or covalent inactivators of cruzain have encompassed structure-based design, high-throughput screening, and virtual screening.[10] The most successful inhibitor developed so far is K11777, which is comprised of a phenylalanyl-homophenylalanyl dipeptide “scaffold” linked to an electrophilic vinyl sulfone warhead that forms an irreversible Michael adduct with the eponymous active-site cysteine (Figure 1).[11] K11777 cures Chagas disease in mouse models and protects dogs from cardiac damage during *T. cruzi* infection.[12] However, preclinical studies of K11777 were halted because of its poor tolerability in primates and dogs even at low doses, which may be attributable to its irreversible mode of inactivation.

While the development of new cruzain inhibitors has been extensive, no detailed studies of the catalytic mechanism of cruzain exist. Sequence analysis and substrate profiling studies indicate that cruzain is a member of the cathepsin L-like papain family and belongs to clan CA of the cysteine proteases.[13,14] The active sites of cysteine proteases contain a catalytic cysteine-histidine “dyad” that exists as either a neutral Cys-SH:His or a thiolate-imidazolium ion pair Cys–S^-:H-His^+ species in the free enzyme. The initial protonation state of this catalytic dyad has been the subject of considerable debate.[15–18] Only recently has the catalytic mechanism of cruzain been investigated by molecular dynamics. In

that study, an imidazolium-thiolate catalytic dyad exists in ligand-free cruzain, and the imidazolium ion of active-site His_{162} protonates the amide nitrogen prior to attack of the thiolate Cys_{25} on the amide carbonyl group.[19] The catalytic mechanism of cysteine proteases involves two discrete half-reactions: the acylation of the active-site cysteine by the scissile carbonyl of the substrate with release of the amine product and the subsequent hydrolysis of the enzyme−peptide thioester (deacylation) to produce the carboxylate product. During acylation, the imidazolium ion of the active-site histidine provides the proton to the leaving amine (Scheme 1). Kinetic and structural analysis of papain is consistent with a Cys-S^-:H-His^+ ion pair in the free enzyme.[20–23] Kinetic studies by Schneck et al. demonstrated that for human cathepsin C, like papain, the thiolate-imidazolium ion pair predominates in the active site (Scheme 1) in which the pK values for the Cys (4.3) and His (6.5) conform to "reverse protonation" of these residues, and the observed inverse solvent kinetic isotope effect for k_{cat}/K_m is consistent with enrichment of the thiolate ion in D_2O in the free enzyme.[24] However, in other cysteine proteases/hydrolases, such as ubiquitin-specific protease 1 (USP1), a neutral Cys-SH:His dyad exists in the free enzyme, as indicated by normal sKIEs, and the binding of its protein substrate induces apparent proton transfer from Cys-SH to the His to initiate catalysis.[25] Here we investigate in detail the catalytic mechanism of cruzain by pH−rate profiles and the measurement of solvent kinetic isotope effects on steady-state and pre-steady-state kinetics of the proteolytic reaction of different dipeptide substrates.

EXPERIMENTAL PROCEDURES

Materials.

HisPur Ni-NTA Superflow Agarose was purchased from ThermoFisher. HiTrap Q Sepharose FF columns were purchased from GE Healthcare. Deuterium oxide (≥99.9% gram atom D) was purchased from Cambridge Isotope Laboratories. Deuterium chloride [35% (w/w), 99% D], sodium acetate, sodium deuterium oxide [40% (w/w), 99% D], TAPSO, TEA, DEA, DEPC, MES, MMTS, disodium EDTA, glycerol, and sucrose were purchased from Sigma-Aldrich. DNase I was purchased from Roche. Z-FR-AMC was purchased from Biotium. Z-RR-AMC and Z-RA-AMC were purchased from Bachem or Enzo. All other chemicals were reagent grade or better and used without further purification.

Enzyme Preparations.

General procedures for cruzain expression, purification, and activation were performed according to published protocols[26] with some modifications.

Protein Expression.—The plasmid encoding the C-terminally truncated procruzain (Δc; GenBank entry M84342.1) was a generous gift from C. S. Craik. The primer 5'-GCCTTGTCAAGGAGGCGGCGAGCTCCGCGGTGGTCGG-3' was used to generate the G208A mutant of cruzain. The sequence of this mutant plasmid was confirmed by Eton Bioscience. ArcticExpress (DE3) cells were used as the expression strain. After inoculation with frozen glycerol stocks of transformed ArcticExpress cells, small cultures (5 mL) of Luria broth containing carbenicillin (100 μg/mL) and gentamycin (20 μg/mL) were grown overnight at 37 °C to saturation. Five milliliters of this starting culture was added to 1 L of

Terrific Broth medium containing the same amount of carbenicillin and gentamycin. After being grown for ~6 h (OD_{600} = 0.6), cultures were moved to 18 °C, and protein expression was initiated by adding 0.4 mM isopropyl β-D-1-thiogalactopyranoside. Cells were harvested after overnight expression, and the cell pellets were stored at −20 °C.

Protein Purification and Activation of Cruzain from Procruzain.—Frozen cell pellets were thawed and resuspended at a concentration of 50 mL/L of growth medium in lysis buffer [50 mM Tris (pH 10), 300 mM NaCl (buffer A), containing 10 mM imidazole, 1 mM $CaCl_2$, 1 mM $MgSO_4$, 1 μM DNase I, 1 mM phenylmethanesulfonyl fluoride (PMSF), and 2 mM methylmethanethiosulfonate (MMTS)]. After resuspension, samples were lysed via sonication (ThermoFisher model FB505 sonicator) with 20 s pulses (50% amplitude) followed by 59 s intervals at 50% amplitude for a 10 min total period of sonication. The resulting lysate was centrifuged at 17000*g* for 1 h. The supernatant was passed through a 0.2 μm filter prior to being loaded onto a HisPur Ni-NTA column (ThermoFisher Scientific) equilibrated with buffer A. After being extensively washed with buffer A containing 50 mM imidazole, bound procruzain was eluted with buffer A containing 500 mM imidazole. MMTS at a final concentration of 5 mM was added to each of the fractions containing His_6-tagged procruzain upon elution.

Fractions containing procruzain were combined and dialyzed overnight at 4 °C against 2 L of activation buffer [50 mM sodium acetate (pH 5.0), 100 mM NaCl, and 0.1 mM disodium EDTA] in the absence of reducing agents. The resulting cloudy solution was transferred into 50 mL conical centrifuge tubes (1 L growth medium per 50 mL activation sample). Autoproteolysis was initiated by addition of 10 mM DTT, followed by incubation at 37 °C for 1–3 h until the dialysate solution became completely clear. The clarified solution was then dialyzed against 50 mM Tris (pH 8.0) to remove salts, and this dialysate was loaded onto two 5 mL HiTrap Q FF columns connected in a series. Cruzain was eluted with 500 mL of 50 mM Tris (pH 8.0) buffer containing a gradient of 50–400 mM NaCl. The resulting cruzain was flash-frozen and stored at −80 °C in the eluant containing 20% glycerol, at a protein concentration of 5 mg/mL. The protein was judged to be homogeneous with >95% purity based on sodium dodecyl sulfate−polyacrylamide gel electrophoresis. The N-terminus of the protein (H_2N-APAAVD) was confirmed by Edman sequencing performed by the Protein Chemistry Laboratory at Texas A&M University. Activation of cruzain fractions required removal of MMTS. This was accomplished by five rounds of spin dialysis versus assay buffer containing 5 mM DTT using a 10000 molecular weight cutoff Amicon centrifuge tube. The final enzyme concentration was determined by absorbance at 280 nm using an ε_{280} value of 60430 M^{-1} cm^{-1} (oxidized Cys) or 59930 M^{-1} cm^{-1} (reduced Cys) calculated from the ProtParam tool available on the Expasy server.[27]

Enzyme Assays.

Unless otherwise noted, all enzyme assays were performed at 25 °C. Initial rates of the peptidolytic reaction catalyzed by cruzain were measured by monitoring the fluorescence generated by cleavage of the dipeptide−AMC bond. Assays were conducted in 96-well plates (Greiner, flat-bottom, clear black plates) in a total volume of 250 μL, containing either 50 mM sodium acetate, 50 mM MES, and 100 mM TEA (pH 3.5–8.0) or 50

mM MES, 50 mM TAPSO, and 100 mM DEA (pH 5.5–9.8), each mixed with 1 mM CHAPS, 1 mM Na_2EDTA (Overlap Buffers), 5 mM DTT, and 2 or 10% (v/v) DMSO. Substrates were dissolved in 100% DMSO and then diluted 10-fold such that when they were added to reaction mixtures, the final DMSO concentration was either 2% (v/v) (as used in the pH studies such that high levels of DMSO would not obscure the acid/base dissociation constants) or 10%. Reactions were initiated via the addition of 5 μL of cruzain (final concentrations of 0.017–3.0 nM). Fluorescence was measured on either a SpectraMax M5 (Molecular Devices) or a Synergy HTX (Biotek, Wisnooki, VT) microplate reader (λ_{ex} = 360 nm; λ_{em} = 460 nm). Initial rates were determined from continuous kinetic time courses and calculated from the earliest time points, typically in <10 min.

pH−rate Profiles.

The pH dependence of k_{cat} and k_{cat}/K_m for cruzain-catalyzed peptidolysis of Z-FR-AMC, Z-RR-AMC, and Z-RA-AMC was investigated at pH 3.5–10 with two different three-component mixed buffer systems. Cruzain was preincubated for 30 min at each pH, after which the pH was readjusted to 7.0 to determine the stability of the enzyme over the experimental pH range. Cruzain activity was unchanged from pH 4.5 to 9.5, affording a wide range for the evaluation of pH−rate profiles. To maintain a constant ionic strength of 0.1, 50 mM sodium acetate/MES and 100 mM TEA were used for pH 3.5–8.0 and 50 mM MES/TAPSO and 100 mM DEA were used for pH 5.5–10.0 (Overlap Buffers);[28] the pH was adjusted with small aliquots of concentrated HCl or NaOH. There were no significant differences in values of k_{cat} and K_m at the overlap pH points for the two buffers. Typical enzyme concentrations (wild type) used in kinetic measurements were 17 pM, 0.17–1.7 nM, and 1–70 nM for Z-FR-AMC, Z-RR-AMC, and Z-RA-AMC, respectively. Concentrations for the E208A mutant of cruzain used in kinetic measurements were 17 pM, 3.4–34 nM, and 20–1400 nM for Z-FR-AMC, Z-RR-AMC, and Z-RA-AMC, respectively. The temperature dependence of the k_{cat}/K_m of wild-type (WT) cruzain was determined in a single mixed buffer of 50 mM MES/TAPSO, 100 mM DEA, 1 mM Na_2EDTA, and 1 mM CHAPS (pH 4.5–7.5) at 25–40 °C. The apparent pH for the buffer was determined at each temperature used, and data for $\log k_{cat}/K_m$ versus pH were corrected for a diminution in pH of 0.012 unit/°C.

Solvent Kinetic Isotope Effects.

To determine the solvent kinetic isotope effects of cruzain substrates, Overlap Buffers were prepared in 100% D_2O and adjusted to the desired pD using either sodium deuteroxide or deuterium chloride (pD 3.5–10). The calculated final percentage of deuterium in these buffers was 93%, based on precedent.[24] pD values were determined as the measured pH value + 0.4.[29] Values of k_{cat} and k_{cat}/K_m for Z-FR-AMC, Z-RR-AMC, and Z-RA-AMC were acquired from initial rate studies in deuterated Overlap Buffers also containing 5 mM DTT and 2% DMSO. Solvent kinetic isotope effects were then ascertained from comparison of the pH- and pD-independent values of these kinetic parameters as described in Data Analysis. To rule out any viscosity effect of D_2O on the initial rate, the kinetic parameters k_{cat} and k_{cat}/K_m were measured with 0.5–100 μM Z-FR-AMC in Overlap Buffers containing 5 mM DTT, 10% DMSO, and either 0–25% (w/v) sucrose or 0–12% (w/v) glycerol.

Inactivation of Cruzain by Iodoacetamide and Diethylpyrocarbonate.

WT cruzain (1–3 nM) was preincubated for 0–80 min with 0–1 mM iodoacetamide at pH 5.5–10 in 50 mM MES, 50 mM TAPSO, 100 mM DEA, and 10% DMSO. Because DTT reacts with iodoacetamide and potentially with DEPC, it was omitted from the preincubation and assay mixtures. Likewise, 1–3 nM WT cruzain was preincubated for 0–5 min with 0–100 μM DEPC (dissolved in either 100% DMSO or ice-cold ethanol) at pH 5.5–10 in 50 mM MES, 50 mM TAPSO, 100 mM DEA, and 10% DMSO. Aliquots (5 μL) of both types of preincubation mixtures were diluted into 250 μL assay mixtures containing Overlap Buffers (pH 7.5) and 10 μM Z-FR-AMC [10% (v/v) DMSO], and residual cruzain activity was measured.

Pre-Steady-State Kinetics.

Pre-steady-state kinetics for cruzain-catalyzed reactions of 0.5–10 μM Z-FR-AMC and 1.6–60 μM Z-RR-AMC were conducted at 25 °C and pH(D) 7.5. Time courses (0.002–0.2 s) of AMC production were measured using a Kintek AutoSF-120 stopped-flow fluorimeter (Kintek, Snow Shoe, PA), where fluorescence readings of AMC (excitation at 348 nm and emission at 438 nm with a 400 nm cutoff filter) were collected and analyzed by Kintek software. Reaction mixtures contained 50 mM MES, 50 mM TAPSO, 100 mM DEA, 1 mM CHAPS, and 1 mM Na_2EDTA and were prepared in either H_2O or D_2O. Solutions of WT cruzain (0.5 μM) and the substrate were loaded into separated syringes that each contained buffer, 10% DMSO, and 5 mM DTT. Fluorescence time courses were comprised of 1000 time points for each fixed substrate concentration, and time courses of AMC formation (millivolts) were converted to nanomolar concentrations of product formed following calibration of the system with known concentrations of AMC. Calibration of the stopped-flow fluorimeter was ascertained by measurement of the concentration of free AMC found in each solution of substrate, and two kinetic traces were generated: one background trace measuring the signal of the contaminating free AMC present in the substrate and one reaction trace monitoring the newly generated AMC from the cleavage of the peptide substrate by cruzain. After the background had been subtracted, the voltage signals were converted into concentration according to a calibration curve generated from solutions containing known concentrations of AMC. Separate experiments were conducted to determine the binding constant (K_{ia}) for both substrates in H_2O and D_2O using a larger range of substrate concentrations (0–80 μM).

Data Analysis.

Values of k_{cat} and K_m for cruzain-catalyzed reactions of the fluorogenic peptide substrates were determined by nonlinear least-squares fits of the initial velocity data to eq 1 using GraphPad Prism 6.0 or SigmaPlot 12.0 (Systat, Inc.). For eq 1, k_{cat} is the turnover number, E_t is the concentration of active sites of cruzain, and K_a is the Michaelis constant for substrate A.

$$\frac{v}{E_t} = \frac{k_{cat}[A]}{K_a + [A]} \quad (1)$$

In enzyme inactivation studies using affinity agents, residual cruzain activity (v_i/v_0) plotted against time (eq 2) was used to obtain pseudo-first-order rate constants of inactivation (k_{obs}) at each inactivator concentration (I). The second-order rate constants, k_{inact}/K_I, for inactivation of cruzain by iodoacetamide were determined from the slopes of the replots of the pseudo-first-order rate constants versus iodoacetamide concentration, as fitted to eq 3a. Similarly, for DEPC, values of k_{obs} versus time were fitted to eq 3b, and for both equations, k_{inact} and K_I are the maximal rate of inactivation and the concentration of inactivator at which the rate of inactivation is half that of k_{inact}, respectively.

$$\ln\left(\frac{v_i}{v_0}\right) = -k_{obs}t \tag{2}$$

$$k_{obs} = \left(\frac{k_{inact}}{K_I}\right)[I] \tag{3a}$$

$$k_{obs} = \frac{k_{inact}[I]}{K_I + [I]} \tag{3b}$$

Data for all pH profiles were fitted as semilogarithmic plots to eq 4

$$y = \frac{c}{1 + 10^{(pK_1 - pH)} + 10^{(pH - pK_2)}} \tag{4}$$

where y is the observed kinetic parameter k_{cat}/K_m or k_{cat}, c is the pH-independent value of y, and pK_1 and pK_2 are the apparent acid and base dissociation constants, respectively. For plots of k_{cat}/K_m versus pH(D) in which a "hollow" was observed, rather than apparent slopes of 1 and −1 characteristic of "bell-shaped" curves (eq 4), data were fitted to eq 5

$$\frac{k_{cat}}{K_m} = \frac{c\left(1 + 10^{(pK_a - pH)}\right)}{\left(1 + 10^{(pK_1 - pH)}\right)\left(1 + \frac{10^{(pK_a - pH)}}{\beta}\right)} \tag{5}$$

where c is the pH-independent value of k_{cat}/K_m, $K_a = \alpha K_1$, where α is a collection of rate constants, K_1 is the apparent acid dissociation constant, and β is a collection of rate constants that comprise the "stickiness ratio" for the substrate.[30]

The solvent kinetic isotope effects (sKIEs, E_C) were calculated using eq 6

$$E_C = \frac{\frac{c_H}{c_D} - 1}{F_i} \tag{6}$$

where c_H and c_D are pH(D)-independent values of k_{cat}/K_a or k_{cat} and F_i is the fraction of D_2O used in the studies. Error propagation on calculated values of the sKIEs was determined from the ratios of the experimental values in H_2O and D_2O, by the use of eq 7

$$\text{error propagation} = \delta c_{\mathrm{H}}\left(\frac{\partial f}{\partial c_{\mathrm{H}}}\right) + \delta c_{\mathrm{D}}\left(\frac{\partial f}{\partial c_{\mathrm{D}}}\right) + \delta c_{F_i}\left(\frac{\partial f}{\partial c_{F_i}}\right) \tag{7}$$

where δc_{H}, δc_{D}, and δc_{F_i} are experimental standard deviations of c_{H}, c_{D}, and c_{F_i}, respectively, and $\partial f/\partial c_{\mathrm{H}}$, $\partial f/\partial c_{\mathrm{D}}$, and $\partial f/\partial c_{F_i}$ are the respective partial derivatives of eq 6.

Pre-steady-state data were fitted to a single-exponential function (eq 8) for each fixed concentration of Z-FR-AMC and Z-RR-AMC. In eq 8, P is product AMC formed (bound or free, micromolar), v_{ss} is the apparent steady-state rate, t is the time in seconds, β is the apparent burst amplitude, λ is the apparent rate of the exponential phase, and C is a constant of calibration.[24] Steady-state rates, burst amplitudes, and transient rate constants were replotted at each concentration of substrate ([A]) using eqs 1,9, and 10, respectively, for which β is the burst amplitude (micromolar), λ is the transient rate constant (inverse seconds), k_{cat} is the steady-state turnover number (inverse seconds), k_{ac} and k_{dac} are the apparent rate constants of the acylation and deacylation half-reactions, respectively (inverse seconds), E_{t} is the cruzain concentration (micro-molar), and K_{a} and K_{ia} are the Michaelis and dissociation constants of the substrate, respectively.

$$P = v_{\mathrm{ss}}t + \beta\left(1 - \mathrm{e}^{-\lambda t}\right) + C \tag{8}$$

$$\beta = \left[\frac{k_{\mathrm{cat}}[\mathrm{A}]}{k_{\mathrm{dac}}(K_{\mathrm{a}} + [\mathrm{A}])}\right]^2 E_{\mathrm{t}} \tag{9}$$

$$\lambda = \frac{(k_{\mathrm{ac}} + k_{\mathrm{dac}})[\mathrm{A}] + k_{\mathrm{dac}}K_{\mathrm{ia}}}{K_{\mathrm{ia}} + [\mathrm{A}]} \tag{10}$$

$$P = \frac{k_{\mathrm{cat}}E_{\mathrm{t}}[\mathrm{A}]}{K_{\mathrm{a}} + [\mathrm{A}]}t + \left[\frac{k_{\mathrm{cat}}[\mathrm{A}]}{k_{\mathrm{dac}}(K_{\mathrm{a}} + [\mathrm{A}])}\right]^2 E_{\mathrm{t}} \left\{1 - e^{-\left[\frac{(k_{\mathrm{ac}} + k_{\mathrm{dac}})[\mathrm{A}] + k_{\mathrm{dac}}K_{\mathrm{ia}}}{K_{\mathrm{ia}} + [\mathrm{A}]}\right]}\right\} + C \tag{11}$$

Additionally, pre-steady-state data conforming to a singleexponential function were fitted globally to eq 11, in which more than 10000 data points representing pre-steady-state time courses for all fixed concentrations of Z-FR-AMC or Z-RR-AMC were simultaneously fitted. In all cases, the most appropriate fit for each equation was determined by an F-test analysis of the results of nonlinear regression.

Nomenclature.

Isotope effects are expressed using the notation of Cook, Cleland, and Northrop.[31,32] Solvent kinetic and equilibrium isotope effects measured on k_{cat}, $k_{\mathrm{cat}}/K_{\mathrm{a}}$, and other kinetic parameters are notated as leading superscripts, designated as “D” for the sake of simplicity, with the variable substrate as the right subscript.

RESULTS AND DISCUSSION

Steady-State Kinetics and Substrate Specificity.

Initial velocity data for the three fluorogenic dipeptide substrates are summarized in Table 1. The value of k_{cat} is largest for Z-FR-AMC (17 s^{-1}), which is more than twice than that of Z-RR-AMC, suggesting a better accommodation for a Phe residue at the P2[33] position than for Arg. The possibility that cruzain may accommodate both Phe and Arg at the P_2 position of dipeptide substrates has been attributed to the role of Glu_{208} found in the S_2 binding subsite (Figure 1). It was shown from structural studies that Glu_{208} points toward a P_2 Arg residue on the substrate but away from Phe in the P_2 position of the substrate, as depicted in Figure 1, for which the irreversible inactivator K11777 (*N*-methyl-piperazine-Phe-homoPhe-vinylsulfone-phenyl) contains a phenylalanine as its P_2 residue.[11] The k_{cat} of Z-RA-AMC (0.89 s^{-1}) is nearly 20-fold lower than that of Z-FR-AMC, indicating that a larger residue at the P_1 position is preferred for catalysis, while a hydrophobic residue at P_2 is more favorable than a charged one. Values of k_{cat}/K_m for the three substrates range from 10^4 to 10^7 M^{-1} s^{-1}, wherein k_{cat}/K_m for Z-FR-AMC is 3 orders of magnitude larger than the lowest value of k_{cat}/K_m for Z-RA-AMC. On the basis of the rank order of k_{cat}/K_m values for the three different substrates, cruzain clearly prefers substrates with a large, charged residue at the P_1 position and a hydrophobic residue in the P_2 position, consistent with findings from a comprehensive analysis of peptide substrate specificity.[14]

Mutagenesis of Glu_{208}.

We prepared the E208A mutant of cruzain to investigate the role of this residue in recognition of the P_2 substituent of substrates. For Z-FR-AMC, k_{cat} for WT and E208A cruzain is equivalent, K_m is increased 2.5-fold, and k_{cat}/K_m is halved for the mutant enzyme (Table 1). Accordingly, while the E208A mutant "recognizes" Z-FR-AMC less effectively than wild-type cruzain does, turnover of the substrate is comparable, suggesting that once bound, mutant cruzain processes Z-FR-AMC at rates similar to that of the wild-type enzyme. However, mutation of Glu_{208} exhibited profound effects on all three kinetic parameters of substrates bearing an Arg residue at the P_2 position. Diminutions by 300- and 200-fold in the k_{cat}/K_m values of Z-RR-AMC and Z-RA-AMC, respectively, were observed for the E208A mutant cruzain compared to that of the wild type, suggesting that ion pairing between Glu_{208} and P_2 Arg is essential for recognition of these substrates. This is also reflected in values of K_m, which are increased for Z-RR-AMC (10-fold) and Z-RA-AMC (4-fold). Values of k_{cat} for mutant cruzain, unlike Z-FR-AMC, are greatly diminished for the substrates containing Arg at P_2: Z-RR-AMC (26-fold lower) and Z-RA-AMC (50-fold lower).

pH−rate Profiles.

The pH–rate profiles for Z-FR-AMC, Z-RR-AMC, and Z-RA-AMC with wild-type cruzain over a pH range of 3.5–10.0 are shown in Figure 2 (blue plots) with results summarized in Table 2. For this pH range, there are no prototropic groups on any of the substrates studied. The plot of k_{cat} versus pH (3.5–10.0) for Z-FR-AMC was apparently invariant with pH, while those of Z-RR-AMC and Z-RA-AMC decreased with apparent slopes of +1 and −1

at low and high pH, respectively. When fitting to eq 4 was performed, k_{cat} decreased upon protonation of an enzymatic residue with pK_1 values of 5.5 and 6.1, for Z-RR-AMC and Z-RA-AMC, respectively, and upon deprotonation of an enzymatic residue with a pK_2 of ≥ 10. For Z-FR-AMC, the plot of k_{cat}/K_m versus pH was characterized by a "hollow" as pH decreased, with an apparent slope of less than +1. This plot indicates that Z-FR-AMC is a "sticky" substrate;[30] that is, the substrate desorbs from its Michaelis complex at a rate equal to or less than that of its progression through catalysis.

This result is unsurprising given that the value of k_{cat}/K_m for Z-FR-AMC is near the limit of diffusion control (2.4×10^7 $M^{-1}s^{-1}$), and the pH independence of the values of k_{cat}. For sticky substrates, apparent values of pK are perturbed in plots of k_{cat}/K_m versus pH, resulting in "hollows" in the plots, and do not reflect the true acid or base dissociation constants of the enzymatic residues involved in binding and catalysis.[30] However, fitting of these data to eq 5 uncovered a pK_1 value of 6.2 associated with an enzymatic group that must be unprotonated for substrate binding. In contrast, the plots of k_{cat}/K_m versus pH for Z-RR-AMC and Z-RA-AMC exhibited apparent slopes of +1 and −1 at low and high pH, respectively. Fitting of plots of k_{cat}/K_m versus pH to eq 4 resulted in pK_1 values of 6.6 and 6.2 for Z-RR-AMC and Z-RA-AMC, respectively. The basic dissociation constant, pK_2, while poorly determined at these extreme values of pH, equaled ~10 for both substrates. The current pH profiles are similar to those previously reported for cruzain in which pH–rate profiles were also substrate-dependent.[34]

Scheme 2 describes a model for the pH−rate profiles for wild-type cruzain. HE is the monoprotonated form of cruzain to which all three substrates bind (k_1) to form the competent Michaelis complex HEA, which proceeds (k_{ac}) to form the thioester form of cruzain (F), followed by deacylation (k_{dac}) to regenerate the free enzyme. Plots of k_{cat}/K_m versus pH report on the rate of the acylation half-reaction, measure the enzymatic rate at substrate concentrations approaching zero, and describe the protonation state of free enzyme HE. Here, protonation of an enzymatic group with a pK_1 of ~6 or deprotonation of the enzymatic group with a pK_2 of ~10 produces HEH^+ or E^-, respectively, each of which is incapable of catalysis. However, a sticky substrate (A) may also bind to HEH^+(k_7), and with loss of a proton (k_5) from the group of pK_1, the resulting HEA complex is catalytically competent.[30,35] In addition, for a sticky substrate, the proton of the HEA complex may not be subject to removal at high pH such that k_{cat} is apparently independent of pH. The "hollow" observed for the plot of $k_{cat}/K_{Z\text{-}FR\text{-}AMC}$ versus pH arises from protonation of the HEA complex (k_6), and the flattening of the curve is due to perturbation of the value of pK_1 where $K_a = (k_1/k_2)(1 + k_8/k_5)K_1$.[30,35] Fitting of the plot of $k_{cat}/K_{Z\text{-}FR\text{-}AMC}$ versus pH using eq 5 provided an estimate of the stickiness of the substrate from the parameter $\beta = 1 + k_{ac}/k_2 = 70 \pm 50$, indicating that Z-FR-AMC proceeds to form acylated cruzain ~70 times faster than it desorbs from the HEA complex.

For cruzain, the essential basic group with a pK_1 of 6.2–6.6 could be the active-site histidine, or given the salience of an enzymatic group of pK_1 in the pH–rate profiles of substrates bearing an Arg at the P_2 position, this could reflect a carboxylate group such as that of

Glu_{208}. We therefore investigated the pH dependence of the E208A mutant of cruzain for Z-FR-AMC, Z-RR-AMC, and Z-RA-AMC (Figures S1–S5). The semilogarithmic profile of $k_{cat}/K_{Z\text{-}FR\text{-}AMC}$ versus pH for E208A cruzain was similar to that of the wild type except that the curve exhibited less of a "hollow" than WT cruzain did, suggesting that Z-FR-AMC is a less sticky substrate with the mutant enzyme (Figure S1). For Z-RR-AMC and Z-RA-AMC, the pH−rate profiles indicated that a residue with a pK of ~5.3 and ~6.1, respectively, must be unprotonated for catalysis, and that the pH-independent values of k_{cat} and k_{cat}/K_m are almost 20-fold lower than that of wild-type cruzain (Figures S2 and S3). These results rule out Glu_{208} as the residue corresponding to pK_1.

Solvent Kinetic Isotope Effects under Steady-State Conditions.

Solvent kinetic isotope effects from the kinetic parameters k_{cat} and k_{cat}/K_m were acquired from pD–rate profiles generated under conditions identical to those described above using Overlap Buffers prepared in D_2O. Plots of k_{cat} and k_{cat}/K_m versus pD (Figure 2, red points) were identical in form to their counterparts in water, and each plot had been apparently right-shifted by approximately 0.5–0.8 unit for pK_1, due to the solvent equilibrium isotope effect[29] on enzymatic residues (Table 2). A ΔpK value of 0.5 is typical for all enzymatic residues except cysteine.[29,36] The pK_2 values in both the k_{cat} and k_{cat}/K_m profiles were poorly determined because of the lack of data beyond pD = 10. As in H_2O for Z-FR-AMC, k_{cat} was pD-independent, while k_{cat}/K_m versus pD was best fitted to eq 5 because of the presence of a "hollow" in the profile. In D_2O, the stickiness ratio was half that obtained in H_2O, indicating that a solvent isotope effect on k_{cat}/K_m slowed catalysis with respect to substrate desorption. Solvent kinetic isotope effects were ascertained from the pH(D)-independent values of k_{cat} and k_{cat}/K_m. Normal sKIEs were found for k_{cat} with the following values: $^{D_2O}k_{cat} = 1.88 \pm 0.06$ for Z-FR-AMC, $^{D_2O}k_{cat} = 1.76 \pm 0.06$ for Z-RR-AMC, and $^{D_2O}k_{cat} = 1.73 \pm 0.07$ for Z-RA-AMC. The sKIEs for k_{cat}/K_m were normal and only slightly greater than unity (1.1–1.4) for all three substrates (Table 2). These results differ from the sKIEs observed on cathepsin C[24] and papain,[20–22] both of which exhibited $^{D_2O}k_{cat} \geq 2$ and $^{D_2O}(k_{cat}/K_m) < 1.0$ (discussed below). The kinetic parameters k_{cat} and k_{cat}/K_m were unchanged in the presence of either 0–25% (w/v) sucrose or 0–12% (w/v) glycerol, indicating that the experimental normal sKIEs were not a result of the increased viscosity of D_2O, which is comparable to the viscosity of an aqueous solution of 9% (w/v) glycerol.[37]

Temperature Dependence of pK_1.

The temperature dependence of acid dissociation constants provides an additional method for identification of an enzymatic group due to its distinctive values of enthalpy of ionization. Because the dissociation constant for the enzyme side chain with a pK_1 of 6 could be observed in the plot of $k_{cat}/K_{Z\text{-}RR\text{-}AMC}$ versus pH at 25 °C, we investigated the temperature dependence of pK_1 from plots of $\log(k_{cat}/K_{Z\text{-}RR\text{-}AMC})$ versus pH obtained at 25–40 °C. The resulting average values ($n \geq 2$) of pK_1 decreased from 6.2 ± 0.1 at 25 °C to 5.9 ± 0.1 at 40 °C (corrections for the temperature dependence of pH for the buffer used were applied at each temperature). The plot of pK_1 versus $1/T$ was linear (Figure 3). The temperature dependence of acid dissociation constant pK_1 was fitted to eq 12

$$pK_I = \frac{\Delta H_{ion}}{RT} - \frac{\Delta S_{ion}}{R} \quad (12)$$

where T is the temperature in Kelvin, R is the universal gas constant, and ΔH_{ion} and ΔS_{ion} are the values of enthalpy and entropy of ionization, respectively.

The fitting of the temperature-dependent pK_I data resulted in values of 8.4 ± 0.2 kcal/mol and 10^{-19} cal mol^{-1} K^{-1} for ΔH_{ion} and $\Delta S_{ion,}$ respectively. This value of ΔH_{ion} is consistent with either a cysteine or histidine active-site residue, but not a carboxylic acid. From the plots of log k_{cat} versus pH for Z-RR-AMC, we in kind examined the temperature dependence of pK_I (5.3–5.5). The resulting average values (n ≥ 2) of pK_I decreased from 5.34 ± 0.06 at 25 °C to 4.92 ± 0.06 at 40 °C, and again, fitting of pK_I versus $1/T$ (Kelvin) was linear (Figure 3). Fitting to eq 12 resulted in ΔH_{ion} and ΔS_{ion} values of 7.1 ± 0.06 kcal/mol and 10^{-15} cal mol^{-1} K^{-1}, respectively. The residue involved in the k_{cat} profile is also likely to be a basic histidine.

Affinity Labeling with Iodoacetamide and Diethyl Pyrocarbonate.

We employed affinity labeling studies of cruzain using the thiol-specific reagent, iodoacetamide. Preincubation of iodoacetamide (0–1 mM) with cruzain, followed by its dilution and analysis of residual enzymatic activity, resulted in irreversible, time-dependent inactivation. The observed first-order rate constants of inactivation, k_{obs}, obtained from fitting of residual enzyme activity versus time (eq 2) demonstrated higher rates of inactivation with increasing concentrations of iodoacetamide (Figure 4A). The inclusion of increasing, fixed concentrations of Z-FR-AMC in the reaction mixtures ablated the inactivation, indicating that iodoacetamide reacted with catalytic Cys_{25} (data not shown). A replot of the first-order rate constant of inactivation, k_{obs}, versus iodoacetamide concentration demonstrated that inactivation of cruzain by iodoacetamide was not saturable (Figure 4A), which is typical for affinity labeling agents. The second-order rate constant for inactivation, k_{inact}/K_J, was obtained from the slopes of replots of k_{obs} versus iodoacetamide concentration by fitting to eq 3a (Figure 4A, inset). At pH 8.0, $k_{inact}/K_I = 6.9 \pm 0.2 M^{-1}s^{-1}$.

We determined the pH dependence (Ph 5.5–10.0) of cruzain inactivation by iodoacetamide (Figure 4B). The resulting plot of k_{inact}/K_I versus pH exhibited a “wave” in which the level of enzyme inactivation increased from an invariant value at neutral pH to a higher value of 180 ± 20 M^{-1} s^{-1} at pH 10. The pH dependence of the second-order rate constant of inactivation of cruzain (k_{inact}/K_I) by iodoacetamide can be fitted to eq 13

$$\frac{k_{inact}}{K_I} = \frac{k_L + k_H\left(10^{(pH-pK_a)}\right)}{1 + 10^{(pH-pK_a)}} \quad (13)$$

where k_L and k_H are values of k_{inact}/K_I at low and high pH, respectively, and pK_a is the acid dissociation constant for an enzymatic group. Fitting of the data indicated that deprotonation of an enzymatic group with a pK_a of 9.76 ± 0.04, likely to be the thiol of active-site Cys_{25}, resulted in the increased rate of inactivation at high pH.

Cruzain can also be inactivated by the histidine-specific affinity agent, diethyl pyrocarbonate (DEPC),[38] in a time-dependent manner. At pH 7.2, preincubation of 1 nM cruzain with 1.6–104 μM DEPC for 40–340 s led to an apparent biphasic inactivation of cruzain (Figure 5A). The initial phase ($t < 40\,s$) occurred too rapidly to be measured; at the shortest preincubation time of 40 s, 11–50% of cruzain was already inactivated by respective DEPC concentrations of 6.5–104 μM. The slower second phase of inactivation was observed at 40–340 s. Replotting the k_{obs} (from fitting to eq 2) versus [DEPC] resulted in a hyperbolic plot (Figure 5B), from which fitting of these data to eq 3b provided the following values: $k_{inact} = 0.23 \pm 0.02\,min^{-1}$, $K_I = 7 \pm 1\,\mu M$, and $k_{inact}/K_I = 550\,M^{-1}\,s^{-1}$. Cruzain is therefore exceptionally sensitive to inactivation by DEPC, especially considering the unmeasurable, rapid phase of inactivation (for comparison, $k_{inact}/K_I = 0.75\,M^{-1}\,s^{-1}$ for phosphotriesterase[39]). The biphasic kinetics of DEPC inactivation suggested that either more than a single histidine had been carboethoxylated or a single histidine had been labeled on both of its nitrogens. No pH dependence of the second phase of DEPC inactivation was observed (pH 5–8) Increasing concentrations of Z-FR-AMC in preincubation mixtures containing cruzain and DEPC led to protection from inactivated by DEPC, which indicated that inactivation occurs via covalent modification of the active site of cruzain.

Protonation States of the Catalytic Cysteine and Histidine Groups.

Cysteine proteases/hydrolases universally possess a conserved catalytic Cys-His dyad, for which the catalytic cysteine serves as a nucleophile to effect acyl transfer, while the histidine facilitates the deprotonation of the thiol of the cysteine and the lytic water and provides a proton for the amine product. The active, monoprotonated forms of cysteine proteases that exist at the maxima of bell-shaped pH−rate profiles (HE in Scheme 2) could result from two tautomeric species of the catalytic dyad: a neutral thiol-imidazole (Cys-SH/His) or an ionic thiolate-imidazolium species (Cys-S^-/$HisH^+$). Bednar has measured the thiolate:thiol nucleophilicity ratio to be 10^{10}:1.[40] Polgar showed via pH−rate profiles of the inactivation of papain by haloacetamide that the pK values of the active-site cysteine (4.0) and histidine (8.4) comprised a case of “reverse protonation”,[20] consistent with the sKIE studies of Creighton et al.[21,22] Solvent kinetic isotope effects on k_{cat}/K_m in these studies were inverse, supporting an enrichment of the thiolate species in D_2O arising from a fractionation factor for thiol of 0.45.[24,36] Lewis et al. demonstrated via nuclear magnetic resonance studies of papain that the imidazoliumthiolate form was the predominant species in the unbound enzyme.[23] In kind, detailed sKIE studies of human cathepsin C were consistent with that of papain; that is, the thiolateimidazolium species of the free enzyme predominates in catalysis: $^{D_2O}(k_{cat}/K_m) = 0.71$, $^{D_2O}k_{cat} = 2.76$, $pK_{a(Cys-SH)} = 4.3$, and $pK_{b(His)} = 6.5$.

In contrast, the pH−rate profiles of k_{cat}/K_m for all three cruzain substrates were characterized by essential unprotonated and protonated catalytic groups with $pK_1 = 6.2 - 6.6$ and $pK_2 = 9.8$, respectively, consistent with neutral forms of the His and Cys species at the pH optimum of cruzain. Other studies described herein confirm the assignment of these pKs. (a) Mutagenic replacement of Glu_{208} does not eliminate cruzain activity or the pK_1 observed in the pH−rate profile of Z-RR-AMC. (b) Values of ΔH_{ion} obtained from temperature variation studies for a pK_1 of 6.2 are in agreement with that of a histidine group. (c) The pH

dependence of inactivation of cruzain by the thiol-specific agent iodoacetamide increased upon deprotonation of a residue with a pK_a of 9.76 ± 0.04. (d) An absence of an inverse sKIE on k_{cat}/K_m indicates that Cys_{25} is protonated in the free enzyme. (e) For Z-RR-AMC and Z-RA-AMC, the ΔpK_1 of 0.5–0.8 is consistent with a histidine group, but not a cysteine.[35,36] Also, from the temperature dependence of a pK_1 of 5.3 from $\log k_{cat}$ vs pH, the obtained value of ΔH_{ion} was also consistent with the involvement of a basic histidine despite the low value of its pK. This pK_1 value of 5.3, for which cruzain is saturated with substrate, is identical to the pK value of 5.2–5.3 for His_{162} obtained from nuclear magnetic resonance analysis of cruzain covalently complexed to dipeptide analogue K11777.[26]

The finding of a neutral Cys-His catalytic dyad for free cruzain has several implications. In free cruzain, it is likely that the respective sulfur and nitrogen atoms of Cys_{25} and His_{162} are not sufficiently proximal to allow the formation of the thiolateimidazolium dyad seen in papain and cathepsin C. In addition, the neutral Cys-His dyad of cruzain would be a far poorer catalyst for hydrolysis than the thiolate-imidazolium dyad, and removal of the proton from Cys_{25} would be required upon substrate binding. As stated above, USP1 hydrolase also possesses a neutral Cys-His dyad for which proton transfer apparently occurs upon binding of the large ubiquitinated protein substrate.[25] In the cases of the cysteine hydrolases dimethylarginine dimethylaminohydrolase (DDAH)[41] and protein arginine deiminases 2 (PAD2),[42] it was similarly proposed that the binding of the positively charged substrates facilitates catalysis by depressing the pK_a of the catalytic cysteine to facilitate its deprotonation. Close examination of the crystal structure of PAD2 revealed that Cys_{645} and His_{471} are further separated than the catalytic dyad is in PAD4, a closely related isozyme found to have the thiolate form of the activesite cysteine irrespective of substrate binding. Cruzain may be a member of an apparent subclass of cysteine hydrolases that, possibly because of active-site geometry, has a neutral Cys-His dyad in their ligand-free forms that requires substrate binding to assist proton transfer from His to Cys, as suggested for USP1.[25]

Pre-Steady-State Kinetics and Solvent Isotope Effects.

Pre-steady-state kinetics for the cruzain-catalyzed hydrolysis of Z-FR-AMC and Z-RR-AMC in both H_2O and D_2O were generated at pH(D) 7.5 in a stopped-low fluorimeter by measurement of product AMC. While solvent kinetic isotope effects should be determined over a range of pH(D) values to eliminate the possibility that observed sKIEs are due to the equilibrium isotope effects that perturb pK values of active-site residues, the lack of pH(D) dependence of either substrate between pH(D) 7.0 and 8.0 allows us to assess the sKIEs at pH(D) 7.5. For each substrate concentration in either solvent, all time courses exhibited an initial, rapid burst of AMC, followed by a linear, steady-state rate of AMC product formation (Figure 6, Figure S4, and Table 3). Burst amplitudes increased with increasing fixed concentrations of substrates to apparent saturation. In contrast, no transient burst was observed for Z-RA-AMC. These results are very similar to those of cathepsin C, in which dipeptide-AMC substrates with high k_{cat}/K_m values are characterized by a burst phase in which the transient:steady-state rate ratio was ~ 20:1, while poor substrates displayed no transient bursts.[24,43] In these previous studies, the rate constant of the transient phase (λ)

could be attributed to the acylation half-reaction (k_{ac}) that encompasses the catalytic steps described by k_{cat}/K_m, while the steady-state rate constant (k_{cat}) was equivalent to the rate constant of the deacylation half-reaction (k_{dac}). Likewise, for Z-FR-AMC and Z-RR-AMC, the observed transient rates demonstrated that the rate of transfer of an acyl group to cruzain exceeded the steadystate rate of deacylation, while for the poor substrate Z-RA-AMC, k_{ac} and k_{dac} are comparable, for which no pre-steady-state burst would be observed. For the pre-steady-state kinetics of Z-FR-AMC (Figure 6) and Z-RR-AMC (Figure S4) performed in D_2O, transient bursts were also observed, albeit with slower transient and steady-state rates (data for the substrate Z-RR-AMC are found in the Supporting Information).

For both substrates, the time courses obtained at each fixed concentration of substrate in either solvent were best fitted to a single-exponential function at all concentrations (eq 8), and values for the resulting steady-state rate constant (v_{ss}), burst amplitude (β), and transient rate constant (λ) were replotted separately versus substrate concentration and fitted to eqs 1,9, or 10 (Figure 7 and Figure S5). For both solvents, we determined the transient rate constant λ over a larger range of fixed concentrations of both substrates (≤80 μM) to observe saturation (Figure 7C). The steady-state rate is diminished in D_2O, but more so at higher concentrations of Z-FR-AMC in agreement with kinetics obtained in the steady state (Figure 7A; $^{D_2O}k_{cat} = 2.3$ from fitting to eq 1), as expected, because the steady-state sKIE is larger on k_{cat} than on k_{cat}/K_m. Interestingly, the apparent effect of D_2O on the burst amplitude is to make it larger than that observed in H_2O, which is due to the large differences in fitted values of K_a. Replotting of the transient rate constant (λ) versus [Z-FR-AMC] provided the following values upon fitting to eq 10: $k_{ac} = 233\,s^{-1}$ and $^{D_2O}k_{ac} = 1.4$. The latter value is identical to that which is obtained for the substrate Ser-Tyr-AMC with human cathepsin C.[24]

Kinetic parameters for Z-FR-AMC and Z-RR-AMC, including sKIEs on k_{cat}, k_{ac}, and k_{dac} as obtained from global fitting using eq 11 of pre-steady-state data are listed in Table 3. This full set of kinetic parameters was well-determined, as opposed to those obtained from replots as depicted in Figure 7. For Z-FR-AMC, the rate constant of cruzain acylation ($k_{ac} = 239 \pm 6\,s^{-1}$) was 8-fold higher than the turnover number ($k_{cat} = 30 \pm 0.1\,s^{-1}$) and the equivalent rate constant of deacylation ($k_{dac} = 35 \pm 1\,s^{-1}$). For Z-RR-AMC, these rate constants were lower: $k_{ac} = 64.5 \pm 0.2\,s^{-1}$, which was 4-fold higher than the turnover number ($k_{cat} = 15.2 \pm 0.1\,s^{-1}$) and its similar rate constant of deacylation ($k_{dac} = 19.9 \pm 0.1\,s^{-1}$). The normal sKIEs for k_{cat} for the two substrates [$^{D_2O}k_{cat} = 2.07 \pm 0.02$ (Z-FR-AMC), and $^{D_2O}k_{cat} = 1.61 \pm 0.02$ (Z-RR-AMC)] are comparable to the pL-independent values obtained in the steady-state studies. For both substrates, normal sKIEs were obtained for the rate constants of acylation and deacylation: $^{D_2O}k_{ac} = 1.34 \pm 0.04$ and $^{D_2O}k_{dac} = 2.2 \pm 0.2$ (Z-FR-AMC), and $^{D_2O}k_{ac} = 1.40 \pm 0.01$ and $^{D_2O}k_{dac} = 1.67 \pm 0.02$ (Z-RR-AMC). The fact that $^{D_2O}k_{cat} \sim {}^{D_2O}k_{dac}$ for both substrates provides further evidence that the rate constants of enzyme deacylation determine the turnover numbers. We attribute the differences in measured values of k_{cat} and K_m under steady-state and presteady-state conditions to the increased concentration of DMSO in the latter experiments, as borne out by additional

studies in the steady state where these parameters were obtained in both 2% (v/v) and 10% (v/v) DMSO (data not shown).

Catalytic Mechanism of Cruzain.

Similar to the mechanism of human cathepsin C, the acylation half-reaction of cruzain is significantly faster than deacylation for those substrates with the highest values of k_{cat}/K_m.[43] Where the two enzymes differ is that for cruzain, all solvent kinetic isotope effects are normal, indicating no enrichment of the Cys-S^-:His-H^+ tautomer of the ligand-free enzyme species in D_2O, so the Cys-His catalytic dyad is neutral at the initiation of catalysis. Accordingly, we may consider two catalytic mechanisms for cruzain for which Cys_{25}-SH and His_{162} are both neutral in free enzyme **E** (Figure 8). Binding of substrate to form **EA** facilitates proton transfer from Cys_{25} to His_{162}, at which point the two mechanisms diverge. In mechanism 1 (Figure 8, green box), conformational isomerization of complex **EA** to **EA'** positions Cys_{25}, His_{162}, and the substrate for a concerted reaction of general base-catalyzed proton transfer and attack of the incipient thiolate of Cys_{25} on the scissile amide carbonyl. In mechanism 2 (Figure 8, magenta box), thiolation of the amide carbonyl occurs in two discrete steps. (1) General basecatalyzed proton transfer to His_{162} establishes the imidazoliumthiolate dyad $\left(\mathbf{EA}^{+/-}\right)$, and (2) the resulting thiolate attacks the amide carbonyl to form tetrahedral intermediate **EX**. One expects that the equilibrium isotope effect (EIE) for the formation of the thiolate in $\mathbf{EA}^{+/-}$ from **EA** would be inverse ($^{D}K_{eq3} = 0.45$ as in the case of cathepsin C),[24] which could allow discrimination of these two mechanisms. The acylation half-reaction is then completed upon the collapse of the **EX** intermediate with proton transfer from the imidazolium group to the departing AMC, which completes the transient phase seen in pre-steady-state kinetics. Discrimination of these two potential mechanisms is discussed below. The slower, deacylation half-reaction ($k_{cat} \sim k_{dac}$) is the same for both mechanisms: Neutral His_{162} in the **F** complex deprotonates the lytic water leading to the second tetrahedral intermediate, **FX**, which then collapses to elaborate the carboxylate product and restores Cys_{25} and His_{162} to their neutral forms.

Estimation of the Individual Kinetic Constants and Intrinsic Isotope Effects.

We sought to discriminate between the two proposed catalytic mechanisms by ascertaining values of the individual rate constants and intrinsic isotope effects on the catalytic steps. Expressions for the eight experimental kinetic parameters were derived in the steady state by the method of net rate constants for both mechanisms (eqs 14−21), for which $a - e$, x, and y represent commitment factors.[44] Equations 18a and 20a are for mechanism 1, and eqs 18b and 20b are for mechanism 2.

$$a = k_3/k_2,\ b = k_5/k_4,\ c = k_6/k_7,\ d = k_5/k_7,\ e = k_7/k_9,\ x = k_{13}/k_{12},\ y = k_{13}/k_{15},\ K_{eq3} = k_3/k_4,\ K_{eq11} = k_{11}/k_{12}$$

$$k_{cat}/K_a = (k_5 K_{eq3})/\{K_{ia}[1 + b(1 + a) + c]\} \quad (14)$$

$$k_{cat} = (k_{ac}k_{dac})/(k_{ac} + k_{dac}) \quad (15)$$

$$k_{ac} = (k_5 K_{eq3})/\{1 + b + c + K_{eq3}[1 + c + d(1 + e)]\} \quad (16)$$

$$k_{dac} = (k_{13}K_{eq11})/[1 + x + K_{eq11}(1 + y)] \quad (17)$$

$$D_2O(k_{cat}/K_a) = \left[{}^Dk_5 + b(1 + a) + c\,{}^Dk_7\,{}^DK_{eq5}\right]/\left[1 + b(1 + a) + c\right] \quad (18a)$$

$$D_2O(k_{cat}/K_a) = \left[{}^DK_{eq3} + b({}^Dk_3 + a) + c\,{}^Dk_7\,{}^DK_{eq3}\right]/[1 + b(1 + a) + c] \quad (18b)$$

$$D_2Ok_{cat} = ({}^Dk_{dac}k_{ac} + {}^Dk_{ac}k_{dac})/(k_{ac} + k_{dac}) \quad (19)$$

$$D2Ok_{ac} = \frac{\left[(1 + K_{eq3})\left({}^Dk_5 + c\,{}^Dk_7\,{}^DK_{eq5}\right) + b + K_{eq3}d({}^Dk_7 + e)\right]}{1 + b + c + K_{eq3}[1 + c + d(1 + e)]} \quad (20a)$$

$$D2Ok_{ac} = \frac{[{}^DK_{eq3}({}^Dk_7c + 1) + {}^Dk_3b + K_{eq3}(1 + c\,{}^Dk_7 + d({}^Dk_7 + e)]}{[(1 + b + c + K_{eq3}(1 + c + d(1 + e)]} \quad (20b)$$

$$D_2Ok_{dac} = \left[{}^Dk_{13}\,{}^DK_{eq11} + x\,{}^Dk_{11} + K_{eq11}({}^Dk_{13} + y)\right]/[1 + x + K_{eq11}(1 + y)] \quad (21)$$

To generate estimates of microscopic rate constants and intrinsic isotope effects ($^Dk_3$, etc.) found in the eight measured kinetic parameters (eqs 14−21) acquired for cruzain under presteady-state and steady-state conditions (Tables 2 and 3), we utilized the dynamic simulation capability of Kintek Explorer[45] to iteratively search for and optimize values of $k_1 - k_{15}$ for the two mechanisms in Figure 8 until we generated simulated time courses that superimposed with the experimental data in H_2O for both Z-RR-AMC and Z-FR-AMC. We conducted a similar simulation for the time courses performed in D_2O, and the intrinsic kinetic isotope effects for each catalytic step ($^Dk_1 - {}^Dk_{15}$) were then calculated by dividing each individual rate constant obtained in H_2O by its counterpart obtained in D_2O; for example, $^Dk_3 = k_{3(H_2O)}/k_{3(D_2O)}$. The simulated time courses generated from these "candidate" rate constants are in good agreement with the experimental time courses for both Z-FR-AMC and Z-RR-AMC in H_2O as shown in Figure 9. By calculating the corresponding rate constants $k_1 - k_{15}$ in D_2O by division of each rate constant by its intrinsic isotope effect $[k_{x(D_2O)} = k_{x(H_2O)}/{}^Dk_x]$, we likewise obtained simulated time courses that can be superimposed on the experimental ones obtained in D_2O (Figure 9). The rate constants $k_1 - k_{15}$ and intrinsic kinetic isotope effects ($^Dk_1$, $^Dk_3$, $^Dk_7$, $^Dk_{11}$, and $^Dk_{13}$) in Table 4 comprise reasonable values for mechanism 2. To differentiate between mechanisms 1 and 2 in Figure 8, we reinserted the determined intrinsic values and individual rate constants into eqs 14−21 for both mechanisms 1 and 2 and calculated values for the eight kinetic parameters (Table 4,

calculated kinetic parameters). The calculated kinetic parameters listed in Table 4 are for mechanism 2, where eqs 18b and 20b were used.

From this and for both substrates, the "candidate" microscopic rate constants were more in accord with mechanism 2 than mechanism 1. Experimental and calculated values for both substrates (mechanism 2) agreed within a variation of ≤ 10%, except for k_{cat}/K_m for Z-RR-AMC, indicating that otherwise these candidate values, while not necessarily unique, are reasonable. By calculating kinetic parameters for both substrates for mechanism 1 using the values listed in Table 4 (eqs 18a and 20a; $^{D}k_5 = 1.4$) we obtained $^{D_2O}(k_{cat}/K_m) = 1.3$ and $^{D_2O}k_{ac} = 1.4$, which exhibited poorer agreement with experimental results than with the kinetic parameters calculated for mechanism 2. One would expect the conformational change in the k_3 step of mechanism 1 to be faster than the subsequent chemical k_5 step and to exhibit no solvent KIE. For Z-FR-AMC under mechanism 2, proton transfer in the k_3 step is 4 times faster than that of Z-RR-AMC $\left(k_3 = 400\,s^{-1}\right.$ compared to $k_3 = 100\,s^{-1}$), suggesting that the Cbz-Phe-Arg dipeptide scaffold is more favorable for initiating proton transfer from Cys_{25} to His_{162} than Cbz-Arg-Arg is, and this difference in rate constants accounts for the 4-fold difference observed for k_{ac}. The stickiness of Z-FR-AMC is reflected in the calculated $(k_5/k_4)(1 + k_3/k_2)$ ratio of 9, while it is lower than the value determined from the plot of $\log(k_{cat}/K_m)$ versus pH. This indicates that upon binding of Z-FR-AMC and proton transfer from Cys_{25} to His_{162}, the enzyme–substrate complex $\mathbf{EA}^{+/-}$ is highly committed to further catalytic steps ($k_5/k_4 = 5$), and accordingly, the subsequent attack by the resulting thiolate on the substrate carbonyl carbon to form EX is rapid ($k_5 = 1100\,s^{-1}$). Collapse of tetrahedral intermediate **EX** to form the enzyme–dipeptide thioester FP is very rapid $\left(k_7 = 6000\,s^{-1}\right)$ with a modest intrinsic isotope effect on te proton transfer from His_{162} to the departing amine (AMC) ($^{D}k_7 = 1.2 - 1.3$).

For Z-RR-AMC, the catalytic steps for $k_1 - k_7$ are unsurprisingly slower than those of Z-FR-AMC, possibly because of a favorable ionic interaction of the Arg group at P_2 with Glu_{208}, while Z-RR-AMC has a lower stickiness ratio $(k_5/k_4)(1 + k_3/k_2)$ of 4. As with Z-FR-AMC, the k_3 step ($100\ s^{-1}$) is the slowest in the acylation half-reaction, and the intrinsic KIE of $^{D}k_3 = 1.4$ accounts for $^{D_2O}k_{ac}$. The $k_5 - k_9$ steps are similar, if not identical, in rate to that of Z-FR-AMC. From the simulation, for both substrates, calculated values for $^{D}K_{eq3}$ of 0.6–0.7 (deprotonation of cysteine) and for $^{D}K_{eq11}$ of 1.3 (hydroxide attack on the thioester) were obtained, where the former value ($^{D}K_{eq\,3} = {}^{D}k_3/{}^{D}k_4$) is inverse because $^{D}k_4 > {}^{D}k_3$. These equilibrium isotope effects compare favorably with values calculated from fractionation factors $^{D}K_{eq3} = 0.45$ and $^{D}K_{eq11} = 1$.[30,36]

In the deacylation half-reaction, the determined rate constants indicated that the rates of formation of the tetrahedral complex for both substrates in FX $(k_{11} = 280$ and $300\,s^{-1})$ are similar, followed by rate-determining collapse of this intermediate to form the cruzain−carboxylate (EQ) complex ($k_{13} = 55$ and $135\,s^{-1}$), for which the intrinsic kinetic isotope effects of $^{D}k_{13} = 1.4$ and 1.9 for Z-RR-AMC and Z-FR-AMC, respectively, account for the measured values of $^{D_2O}k_{dac}$ and $^{D_2O}k_{cat}$.

CONCLUSIONS

Similar to human cathepsin C, the most efficient substrates of cruzain undergo rapid acylation, which precedes rate-limiting deacylation. However, cruzain differs from papain, cathepsin C, and other cysteine proteases, in that its ligand-free form houses the less reactive, neutral Cys-SH/His dyad, implicit in both its pH–rate profiles and sKIEs of >1. This neutral dyad apparently undergoes proton transfer from the thiol of Cys_{25} only upon substrate binding, which most likely occurs in a stepwise fashion (mechanism 2). That general base deprotonation of Cys_{25} – SH by His_{162} elaborates the fact that the reactive thiolate comprises unusual chemistry for cruzain catalysis. Leinhard and Jencks demonstrated more than 50 years ago that general base deprotonation of thiols was not a feature of their reactions with the carbonyl groups of aldehydes and ketones but rather the thiolate fraction present was the sole reactant.[46] Why then would unliganded cruzain adopt the unreactive Cys-SH:His tautomer and rely on this general base catalytic step to unmask the catalytic $Cys\text{-}S^{-}:HisH^{+}$ upon substrate binding? One is tempted to speculate that this is a feature of stringent substrate specificity in that only those bound substrates that affect the proton transfer step (k_3 of mechanism 2) proceed to peptidolysis.

The rate-limiting steps for these two substrates occur during deacylation of these substrates exhibiting normal sKIEs. The less efficient substrate Z-RA-AMC is devoid of a pre-steadystate burst, suggesting that its diminished ability to induce this proton transfer renders $k_{ac} \sim k_{dac}$. In terms of the future design of peptidomimetic covalent inactivators of cruzain such as K11777, the choice of amino acid residues at the P_1 and P_2 residues may determine whether the dipeptide “scaffold” binds in a fashion that promotes the transfer of the proton on Cys_{25}–SH to His_{162} to elaborate the more nucleophilic Cys_{25} thiolate species, which would then progress to alkylation of the activesite catalytic cysteine by its vinyl sulfone warhead. Our results suggest that a peptidomimetic inactivator bearing a Phe-Arg dipeptide may be more favorable than that with an Arg-Arg or Arg-Ala dipeptide.

Supplementary Material

Refer to Web version on PubMed Central for supplementary material.

ACKNOWLEDGMENTS

The authors thank Professor Charles S. Craik for providing a construct for the expression of cruzain and Dr. Larry Dangott for providing protein sequencing. The authors also thank Professor Ken Johnson for assistance with the use of Kintek Explorer.

Funding

The authors thank Texas A&M AgriLife Research for financial support of this work. This work was also supported by National Institutes of Health Grant R21AI127634.

ABBREVIATIONS

MMTS	methylmethanethiosulfonate
DEPC	diethylpyrocarbonate

DTT	dithiothreitol
DMSO	dimethyl sulfoxide
AMC	7-amino-4-methylcoumarin
Z-FR-AMC	carboxybenzyl-L-phenylalanine-L-arginine-7-amino-4-methylcoumarin
Z-RR-AMC	carboxybenzyl-L-arginine-L-arginine-7-amino-4-methylcoumarin
Z-RA-AMC	carboxybenzyl-L-arginine-L-alanine-7-amino-4-methylcoumarin
EDTA	ethylenediaminetetraacetic acid
CHAPS	3-[3-(cholamidopropyl)dimethylammonio]-1-propanesulfonate
TAPSO	3-{[1,3-dihydroxy-2-(hydroxymethyl)-propan-2-yl] amino}-2-hydroxypropane-1-sulfonic acid
MES	2-(*N*-morpholino)ethanesulfonic acid
TEA	triethanolamine
DEA	diethanolamine
sKIE	solvent kinetic isotope effect

REFERENCES

(1). Coura JR, and Vinas PA (2010) Chagas disease: a new worldwide challenge. Nature 465, S6–S7. [PubMed: 20571554]

(2). Hotez PJ, Bottazzi ME, Franco-Paredes C, Ault SK, and Periago MR (2008) The neglected tropical diseases of Latin America and the Caribbean: a review of disease burden and distribution and a roadmap for control and elimination. PLoS Neglected Trop. Dis 2, e300.

(3). Wilkinson SR, and Kelly JM (2009) Trypanocidal drugs: mechanisms, resistance and new targets. Expert Rev. Mol. Med 11, e31. [PubMed: 19863838]

(4). Meirelles MN, Juliano L, Carmona E, Silva SG, Costa EM, Murta AC, and Scharfstein J (1992) Inhibitors of the major cysteinyl proteinase (GP57/51) impair host cell invasion and arrest the intracellular development of Trypanosoma cruzi in vitro. Mol. Biochem. Parasitol 52, 175–184. [PubMed: 1620157]

(5). Harth G, Andrews N, Mills AA, Engel JC, Smith R, and McKerrow JH (1993) Peptide-fluoromethyl ketones arrest intracellular replication and intercellular transmission of Trypanosoma cruzi. Mol. Biochem. Parasitol 58, 17–24. [PubMed: 8459830]

(6). Engel JC, Doyle PS, Hsieh I, and McKerrow JH (1998) Cysteine protease inhibitors cure an experimental *Trypanosoma cruzi* infection. J. Exp. Med 188, 725–734. [PubMed: 9705954]

(7). Doyle PS, Zhou YM, Engel JC, and McKerrow JH (2007) A cysteine protease inhibitor cures Chagas' disease in an immunodeficient-mouse model of infection,. Antimicrob. Agents Chemother 51, 3932–3939. [PubMed: 17698625]

(8). Doyle PS, Zhou YM, Hsieh I, Greenbaum DC, McKerrow JH, and Engel JC (2011) The *Trypanosoma cruzi* protease cruzain mediates immune evasion,. PLoS Pathog. 7, e1002139. [PubMed: 21909255]

(9). Ferrao PM, d'Avila-Levy CM, Araujo-Jorge TC, Degrave WM, Gonçalves A. d. S., Garzoni LR, Lima AP, Feige JJ, Bailly S, Mendonca-Lima L, and Waghabi MC (2015) Cruzipain Activates

Latent TGF-beta from Host Cells during T. *cruzi* Invasion. PLoS *One* 10, e0124832. [PubMed: 25938232]

(10). Martinez-Mayorga K, Byler KG, Ramirez-Hernandez AI, and Terrazas-Alvares DE (2015) Cruzain inhibitors: efforts made, current leads and a structural outlook of new hits. Drug Discovery Today 20, 890–898. [PubMed: 25697479]

(11). Kerr ID, Lee JH, Farady CJ, Marion R, Rickert M, Sajid M, Pandey KC, Caffrey CR, Legac J, Hansell E, McKerrow JH, Craik CS, Rosenthal PJ, and Brinen LS (2009) Vinyl sulfones as antiparasitic agents and a structural basis for drug design. J. Biol. Chem 284, 25697–25703. [PubMed: 19620707]

(12). Barr SC, Warner KL, Kornreic BG, Piscitelli J, Wolfe A, Benet L, and McKerrow JH (2005) A cysteine protease inhibitor protects dogs from cardiac damage during infection by Trypanosoma cruzi. Antimicrob. Agents Chemother 49, 5160–5161. [PubMed: 16304193]

(13). Lecaille F, Kaleta J, and Bromme D (2002) Human and parasitic papain-like cysteine proteases: their role in physiology and pathology and recent developments in inhibitor design. Chem. Rev 102,4459–4488. [PubMed: 12475197]

(14). Choe Y, Leonetti F, Greenbaum DC, Lecaille F, Bogyo M, Bromme D, Ellman JA, and Craik CS (2006) Substrate profiling of cysteine proteases using a combinatorial peptide library identifies functionally unique specificities. J. Biol. Chem 281, 1282412832.

(15). Storer AC, and Menard R (1994) Catalytic mechanism in papain family of cysteine peptidases. Methods Enzymol. 244, 486–500. [PubMed: 7845227]

(16). Shokhen M, Khazanov N, and Albeck A (2009) Challenging a paradigm: theoretical calculations of the protonation state of the Cys25-His 159 catalytic diad in free papain. Proteins: Struct., Funct., Genet 77, 916–926. [PubMed: 19688822]

(17). Solowiej J, Thomson JA, Ryan K, Luo C, He M, Lou J, and Murray BW (2008) Steady-state and pre-steady-state kinetic evaluation of severe acute respiratory syndrome coronavirus (SARS-CoV) 3CLpro cysteine protease: development of an ion-pair model for catalysis. Biochemistry 47, 2617–2630. [PubMed: 18237196]

(18). Paasche A, Zipper A, Schafer S, Ziebuhr J, Schirmeister T, and Engels B (2014) Evidence for substrate binding-induced zwitterion formation in the catalytic Cys-His dyad of the SARS-CoV main protease. Biochemistry 53, 5930–5946. [PubMed: 25196915]

(19). Arafet K, Ferrer S, and Moliner V (2017) Computational Study of the Catalytic Mechanism of the Cruzain Cysteine Protease. ACS Catal. 7, 1207–1215.

(20). Polgar L (1974) Mercaptide-imidazolium ion-pair: the reactive nucleophile in papain catalysis. FEBS Lett. 47, 15–18. [PubMed: 4426388]

(21). Creighton DJ, Gessouroun MS, and Heapes JM (1980) Is the thiolate−imidazolium ion pair the catalytically important form of papain? FEBS Lett. 110, 319–322. [PubMed: 7371836]

(22). Creighton DJ, and Schamp DJ (1980) Solvent isotope effects on tautomerization equilibria of papain and model thiolamines. FEBS Lett. 110, 313–318. [PubMed: 7371835]

(23). Lewis SD, Johnson FA, and Shafer JA (1976) Potentiometric determination of ionizations at the active site of papain. Biochemistry 15, 5009–5017. [PubMed: 10964]

(24). Schneck JL, Villa JP, McDevitt P, McQueney MS, Thrall SH, and Meek TD (2008) Chemical mechanism of a cysteine protease, cathepsin C, as revealed by integration of both steady-state and pre-steady-state solvent kinetic isotope effects. Biochemistry 47, 8697–8710 [PubMed: 18656960]

(25). Villamil MA, Chen J, Liang Q, and Zhuang Z (2012) A noncanonical cysteine protease USP1 is activated through active site modulation by USP1-associated factor 1,. Biochemistry 51, 2829–2839. [PubMed: 22439892]

(26). Lee GM, Balouch E, Goetz DH, Lazic A, McKerrow JH, and Craik CS (2012) Mapping inhibitor binding modes on an active cysteine protease via nuclear magnetic resonance spectroscopy. Biochemistry 51, 10087–10098. [PubMed: 23181936]

(27). Gasteiger E, Hoogland C, Gattiker A, Duvaud S, Wilkins MR, Appel RD, and Bairoch A (2005) Protein identification and analysis tools on the ExPASy server. Proteomics Protocols Handbook, 571–607.

(28). Ellis KJ, and Morrison JF (1982) Buffers of constant ionic strength for studying pH-dependent processes. Methods Enzymol. 87, 405–426. [PubMed: 7176924]

(29). Schowen KB, and Schowen RL (1982) Solvent isotope effects of enzyme systems. Methods Enzymol. 87, 551–606. [PubMed: 6294457]

(30). Cleland WW (1977) Determining the chemical mechanisms of enzyme-catalyzed reactions by kinetic studies. Adv. Enzymol. Relat. Areas Mol. Biol 45, 273–387. [PubMed: 21524]

(31). Cook PF, and Cleland WW (1981) Mechanistic deductions from isotope effects in multireactant enzyme mechanisms. Biochemistry 20, 1790–1796 [PubMed: 7013799]

(32). Northrop DB (1981) The expression of isotope effects on enzyme-catalyzed reactions,. Annu. Rev. Biochem 50, 103–131. [PubMed: 7023356]

(33). Schechter I, and Berger A (1967) On the size of the active site in proteases. I. Papain. Biochem. Biophys. Res. Commun 27, 157–162. [PubMed: 6035483]

(34). Gillmor SA, Craik CS, and Fletterick RJ (1997) Structural determinants of specificity in the cysteine protease cruzain. Protein Sci. 6, 1603–1611. [PubMed: 9260273]

(35). Cleland WW (1982) The use of pH studies to determine chemical mechanisms of enzyme-catalyzed reactions,. Methods Enzymol. 87, 390–405. [PubMed: 7176923]

(36). Quinn DM, and Sutton LD (1991) Theoretical basis and mechanistic utility of solvent isotope effects. In Enzyme Mechanism from Isotope Effects (Cook PF, Ed.) p 73, CRC Press, Inc., Boca Raton, FL.

(37). Karsten WE, Lai C-J, and Cook PF (1995) Inverse solvent isotope effects in the NAD-malic enzyme reaction are the result of the viscosity difference between D_2O and H_2O: implications for solvent isotope effect studies. J. Am. Chem. Soc 117, 5914–5918.

(38). Miles EW (1977) Modification of histidyl residues in proteins by diethylpyrocarbonate. Methods Enzymol. 47, 431–442. [PubMed: 22021]

(39). Dumas DP, and Raushel FM (1990) Chemical and kinetic evidence for an essential histidine in the phosphotriesterase from *Pseudomonas diminuta*. J. Biol. Chem 265, 21498–21503. [PubMed: 2174875]

(40). Bednar RA (1990) Reactivity and pH dependence of thiol conjugation to N-ethylmaleimide: detection of a conformational change in chalcone isomerase. Biochemistry 29, 3684–3690. [PubMed: 2340265]

(41). Stone EM, Costello AL, Tierney DL, and Fast W (2006) Substrate-assisted cysteine deprotonation in the mechanism of dimethylargininase (DDAH) from Pseudomonas aeruginosa. Biochemistry 45, 5618–5630. [PubMed: 16634643]

(42). Dreyton CJ, Knuckley B, Jones JE, Lewallen DM, and Thompson PR (2014) Mechanistic studies of protein arginine deiminase 2: evidence for a substrate-assisted mechanism. Biochemistry 53, 4426–4433. [PubMed: 24989433]

(43). Rubach JK, Cui G, Schneck JL, Taylor AN, Zhao B, Smallwood A, Nevins N, Wisnoski D, Thrall SH, and Meek TD (2012) The amino-acid substituents of dipeptide substrates of cathepsin C can determine the rate-limiting steps of catalysis,. Biochemistry 51, 7551–7568. [PubMed: 22928782]

(44). Cleland WW (1975) Partition analysis and concept of net rate constants as tools in enzyme kinetics. Biochemistry 14, 3220–3224. [PubMed: 1148201]

(45). Johnson KA, Simpson ZB, and Blom T (2009) Global kinetic explorer: a new computer program for dynamic simulation and fitting of kinetic data. Anal. Biochem 387, 20–29. [PubMed: 19154726]

(46). Lienhard GE, and Jencks WP (1966) Thiol addition to the carbonyl group: equilibria and kinetics. J. Am. Chem. Soc 88, 3982–3995. [PubMed: 5915153]

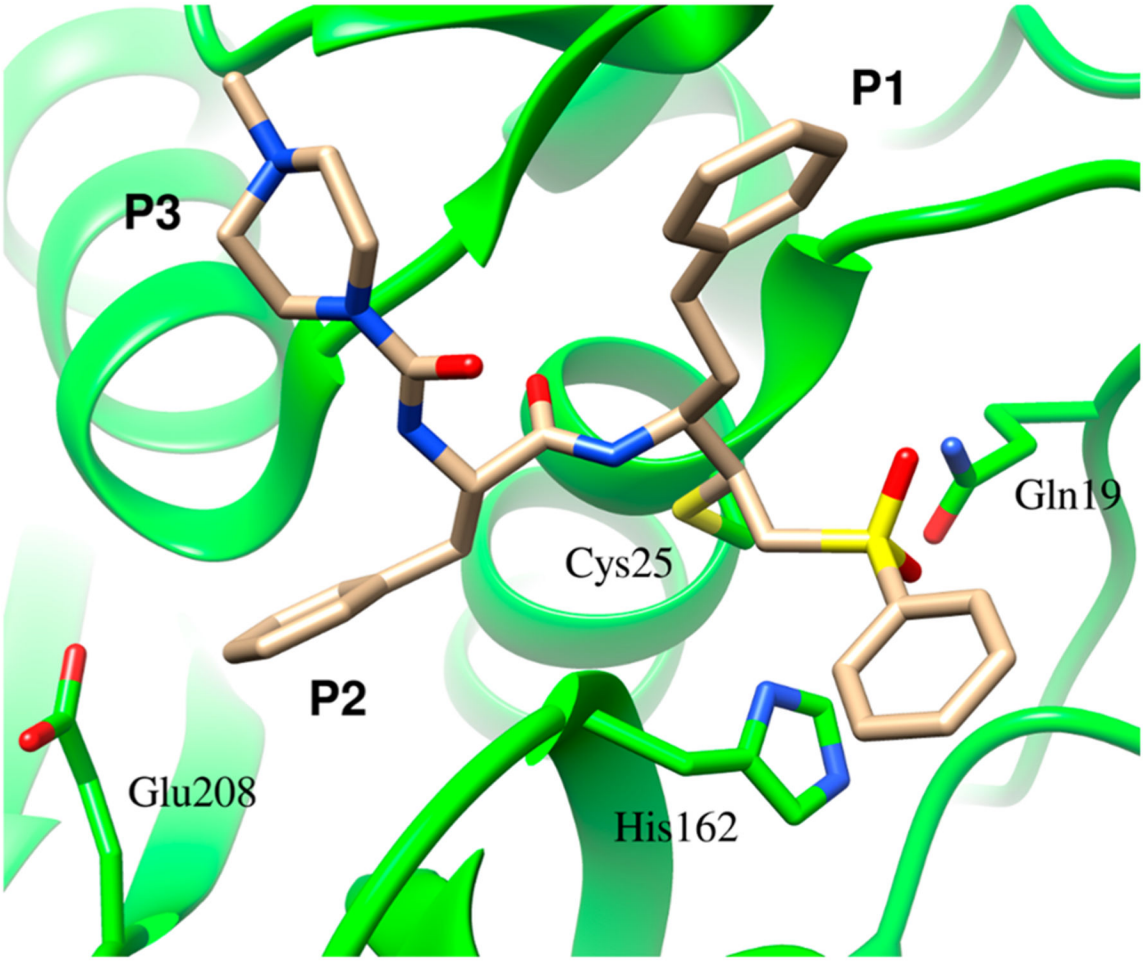

Figure 1.

X-ray crystal structure of cruzain complexed with the irreversible inhibitor K11777, demonstrating the formation of a covalent bond between the active-site Cys_{25} and the α-carbon of the vinyl sulfone warhead.[11] Protein Data Bank entry 2OZ2.

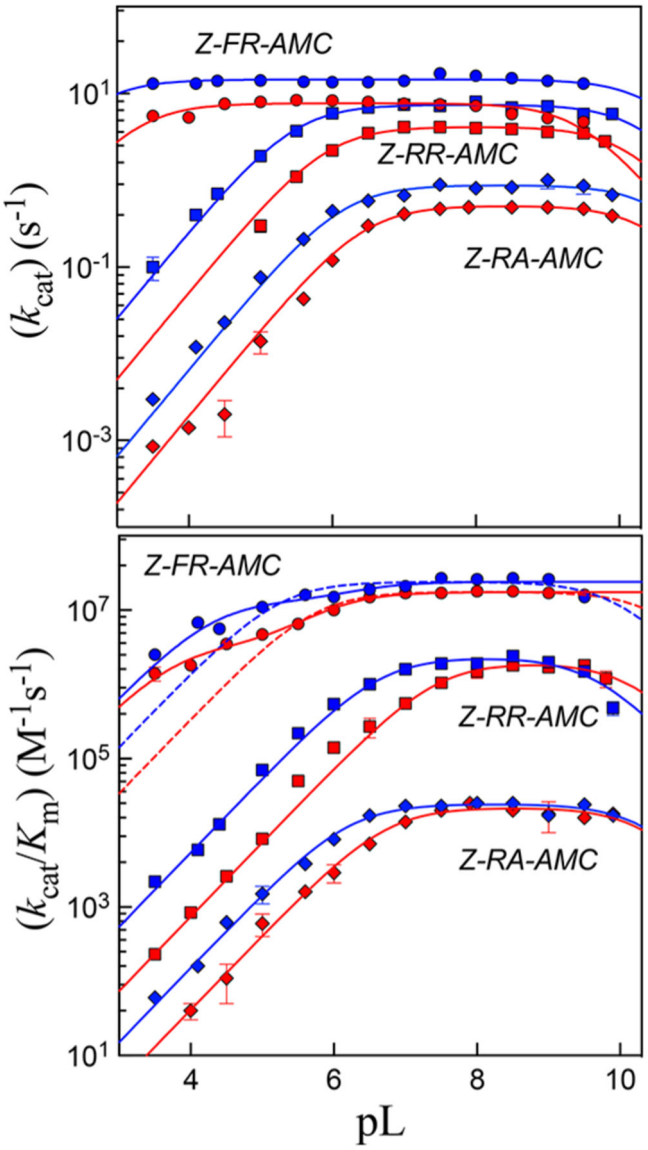

Figure 2.

Plots of pH(D) (pL) rate profiles of k_{cat} (top) and k_{cat}/K_m (bottom) for cruzain-catalyzed hydrolysis of Z-FR-AMC (circles), Z-RR-AMC (squares), and Z-RA-AMC (diamonds). Blue and red symbols are for data obtained in H_2O and D_2O, respectively. Lines drawn through the experimental data of plots of k_{cat} vs pH(D) are from fitting to eq 4, while lines drawn through the experimental data of plots of k_{cat}/K_m vs pH(D) are from fitting to eq 4 (solid line, dashed line for Z-FR-AMC) or eq 5 (solid line for Z-FR-AMC). Error bars represent standard deviations from two independent measurements.

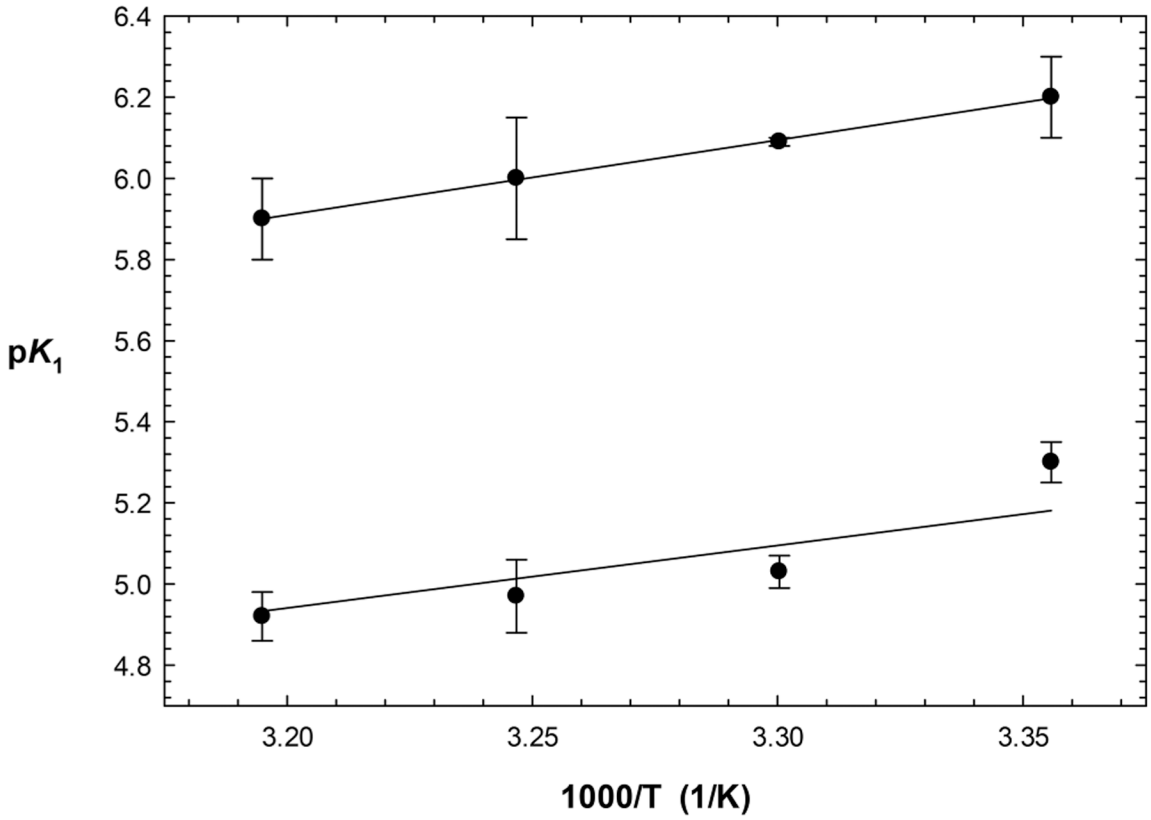

Figure 3.

Effect of temperature on the acid dissociation constant pK_1 from plots of $\log(k_{cat}/K_{Z\text{-}RR\text{-}AMC})$ (top line) and $\log k_{cat}$ (bottom line) vs pH. Values of $pK_1 (n \geq 2)$ vs $1/T$ (Kelvin) were fitted to eq 12, from which ΔH_{ion} values of 8.4 ± 0.2 and 7.1 ± 0.1kcal/mol and a ΔS_{ion} of $0\,cal\,mol^{-1}\,K^{-1}$ were obtained.

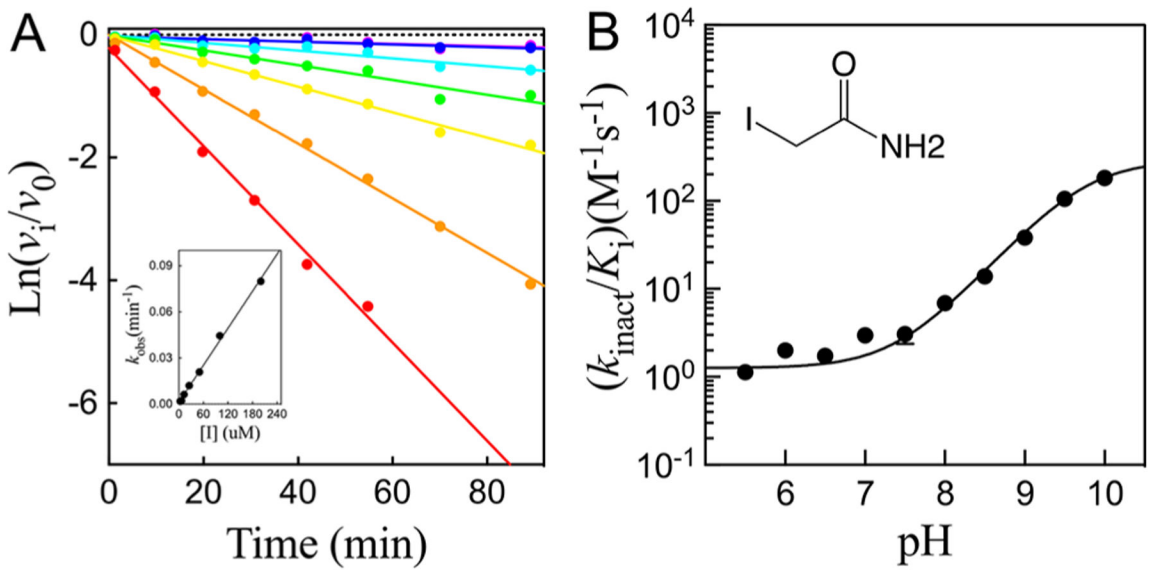

Figure 4.

(A) Representative data of the time-dependent inactivation of cruzain by iodoacetamide at pH 8.0. Lines drawn through the experimental data were from fitting to eq 2. The inset displays a replot of the inactivation rate (k_{obs}) vs iodoacetamide concentration, and the line drawn through the experimental data points was obtained from fitting to eq 3a. (B) pH dependence of the second-order rate constant for cruzain inactivation by iodoacetamide (0–1 mM). The line drawn through the experimental data was obtained by fitting of the data to eq 13.

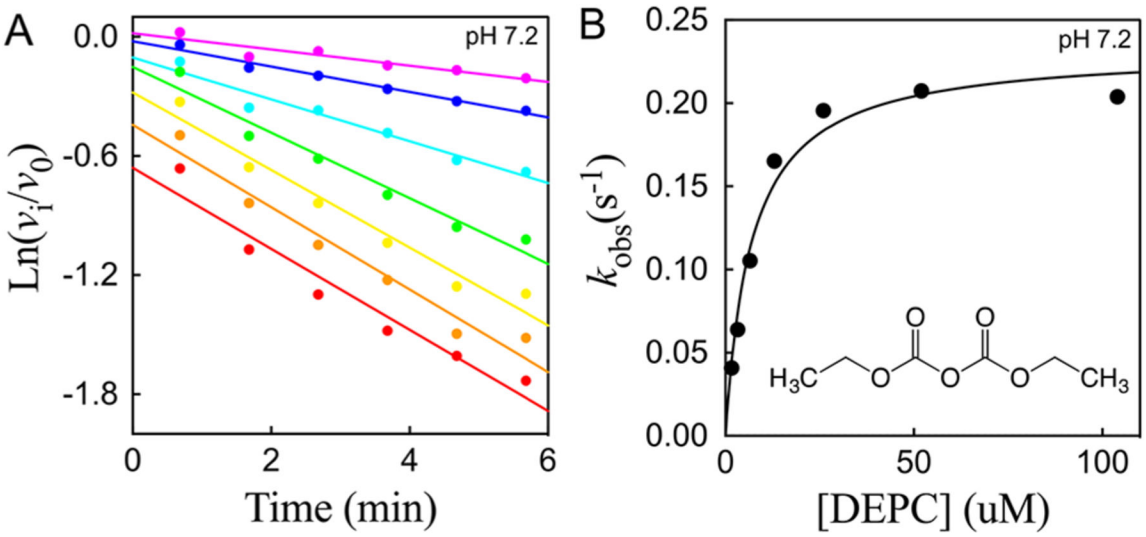

Figure 5.

(A) Time-dependent inactivation of cruzain by 1.6–104 μM DEPC at pH 7.2. The lines drawn through the experimental data points were from fitting of the data to eq 2. (B) Replot of k_{obs}vs [DEPC]. Fitting of the data to eq 3b results in the following values: $k_{inact} = 0.23 \pm 0.02\,\mathrm{min}^{-1}$, $K_I = 7 \pm 1\,\mu$M, and $k_{inact}/K_I = 548\,\mathrm{M}^{-1}\,\mathrm{s}^{-1}$.

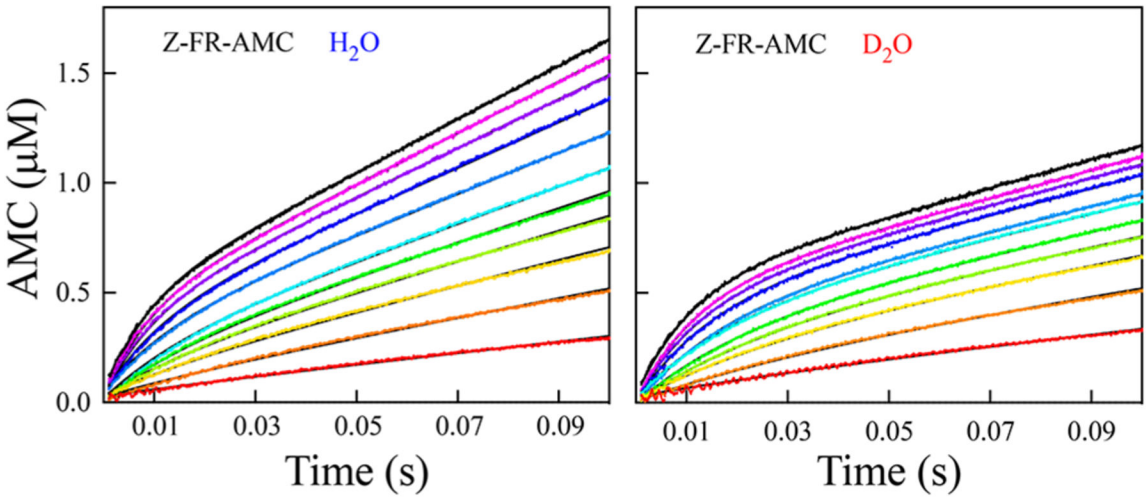

Figure 6.

Pre-steady-state time courses of cruzain-catalyzed hydrolysis of Z-FR-AMC [0.5 (red), 1.0, 1.5, 2.0, 2.5, 3.0, 3.75, 5.0. 6.25, 7.5, and 8.75 (black) μM] in H_2O and D_2O at 0.002–0.1 s, with the product formation shown on the same scale. The black lines drawn through the experimental data represent fitting to eq 11.

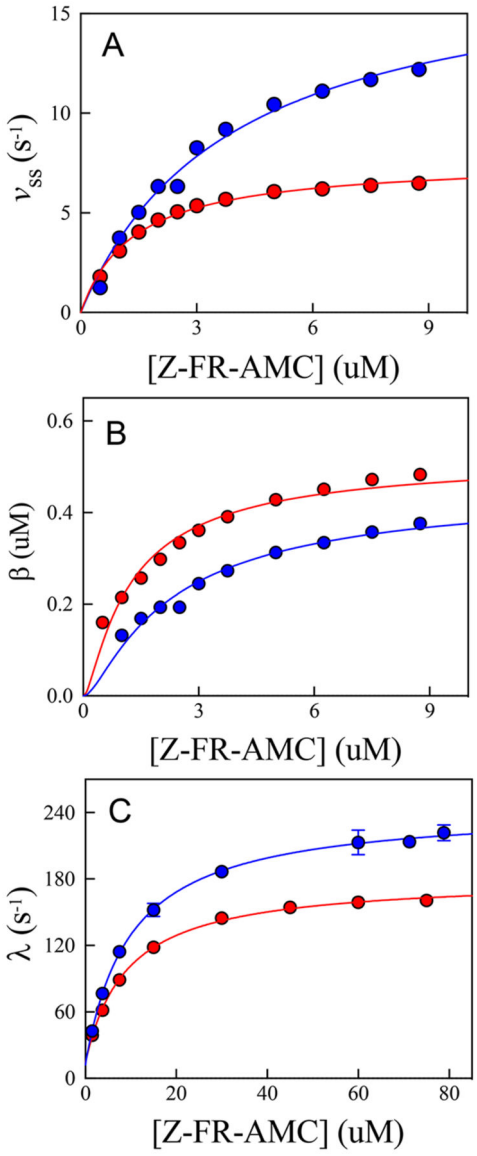

Figure 7.

Replots of the kinetic parameters obtained from fitting individual time courses at each substrate concentration to eqs 8–10 in H_2O (blue) and D_2O (red). Substrate concentrations used to determine the transient rate constants were 1.5–79 μM, compared to substrate concentrations used for the steady-state rate and burst amplitudes (0.5–8.75 μM). (a) Fitting of the steady-state rate vs [Z-FR-AMC] (eq 1) resulted in the following values: $k_{cat} = 34.2 \pm 1.9\,s^{-1}$ and $K_a = 3.9 \pm 0.5\mu$M in H_2O, and $k_{cat} = 14.6 \pm 0.3\,s^{-1}$ and $K_a = 1.4 \pm 0.1\mu$M in D_2O. (b) Fitting of the burst amplitude vs [Z-FR-AMC] (eq 9) resulted in the following values: $k_{cat} = 34\,s^{-1}$, $K_a = 1.1 \pm 0.1\,\mu M$, and $k_{dac} = 36.5 \pm 0.8\,s^{-1}(H_2O)$, and $k_{cat} = 14.6\,s^{-1}$, $K_a = 0.6 \pm 0.06\,\mu$M, and $k_{dac} = 14.4 \pm 0.2\,s^{-1}(D_2O)$. (c) Fitting of the transient rate constant vs [Z-FR-AMC] (eq 10) resulted in the following values: $k_{ac} = 233 \pm 3\,s^{-1}$, $k_{dac} = 12 \pm 3\,s^{-1}$, and $K_{ia} = 9.8 \pm 0.6\,\mu M(H_2O)$, and $k_{ac} = 167 \pm 3\,s^{-1}$, $k_{dac} = 14 \pm 3\,s^{-1}$, and $K_{ia} = 9.0 \pm 0.7\,\mu M(D_2O)$.

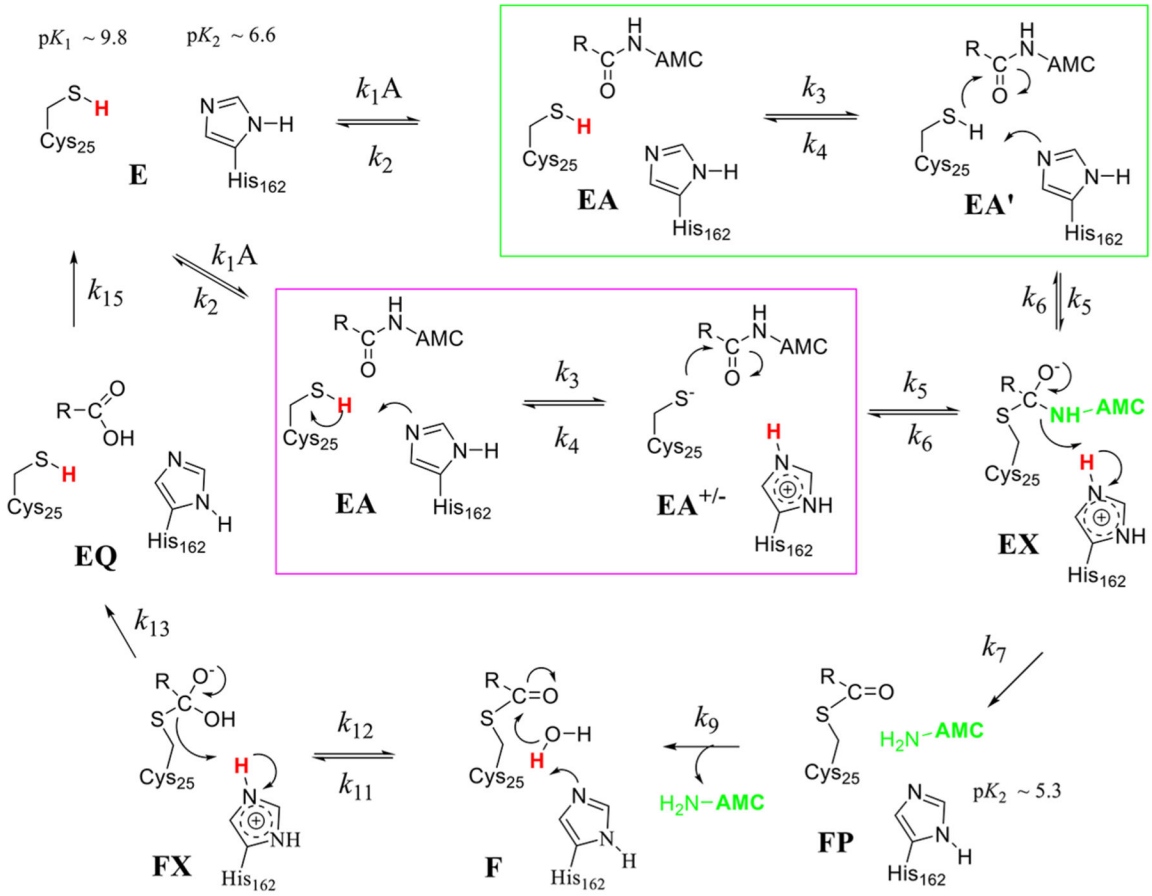

Figure 8.

Proposed catalytic mechanisms for cruzain each involving acylation and deacylation half-reactions. Ligand-free cruzain contains neutral forms of Cys_{25}(pK~9.8) and His_{162}(pK~6.6) that are not positioned for proton transfer until substrate is bound. In mechanism 1 (green box), proton transfer from Cys_{25} to His_{162} is concerted with thiolate attack on the amide carbonyl to form tetrahedral intermediate EX. This occurs in two discrete steps in mechanism 2 (magenta box) in which the thiolate of Cys_{25} attacks the amide. Steps in the deacylation half-reaction are the same for both mechanisms: thio-ester form **F** undergoes attack by a hydroxide ion to form a second tetrahedral intermediate **FX**, which collapses to form the carboxylate product. Protons involved in primary solvent kinetic isotope effects are colored red. Free AMC is colored light green where it is expected to show full fluorescence.

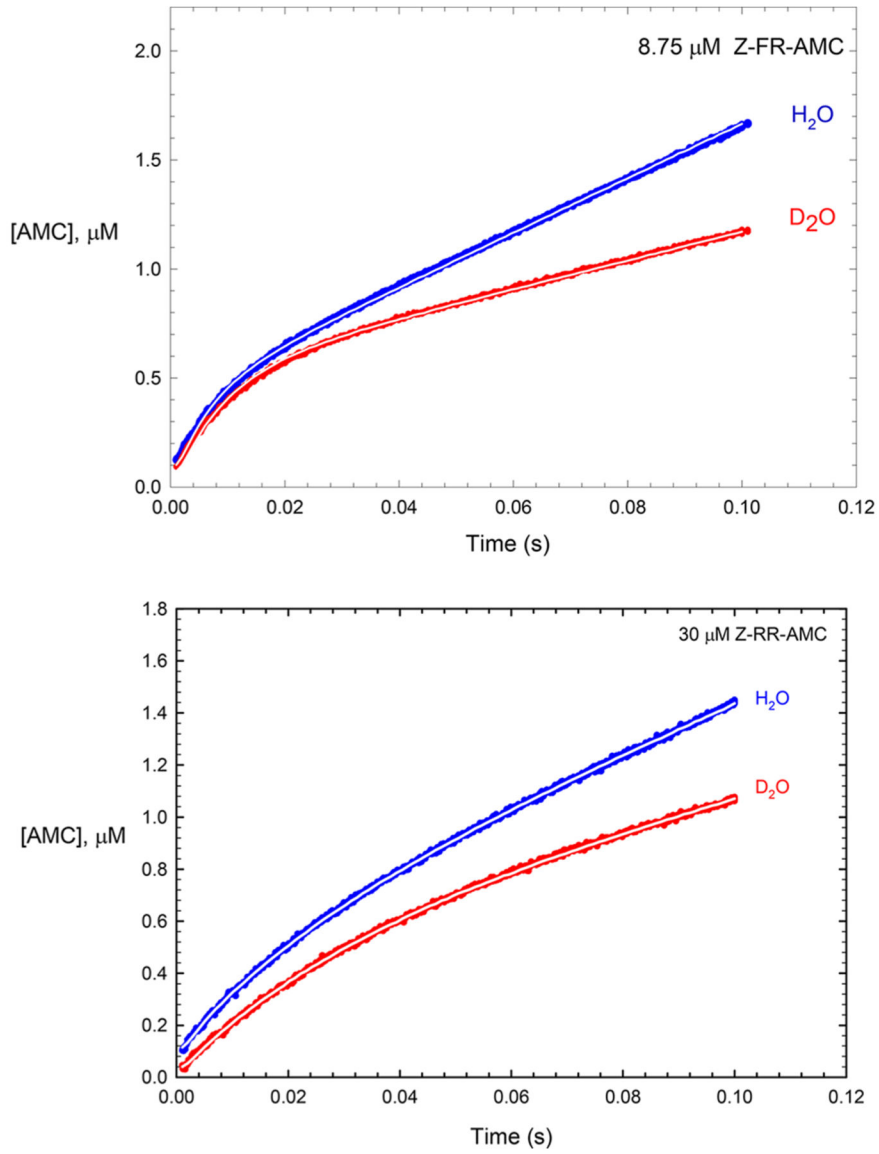

Figure 9.

Experimental pre-steady-state time courses of cruzaincatalyzed hydrolysis of 8.75 μM Z-FR-AMC and 30 μM Z-RR-AMC in H_2O (blue) and D_2O (red) from data found in Figure 6 and Figure S4. The white lines drawn through all curves were produced by dynamic simulation using Kintek Explorer; here the enzyme species EX, FP, and P (P = AMC) and product carboxylic acid were assigned as the observables (generation of a fluorescence signal). For each experimental time course, values of rate constants $k_1 - k_{15}$ were iteratively selected until the simulated curve could be superimposed upon the experimental time course for both substrates, as shown here. The rate constants from this approach led to the "candidate values" listed in Table 4. Values of the intrinsic isotope effects in Table 4 were obtained by dividing each individual rate constant optimized in H_2O by that optimized in D_2O; for example, $^{D}k_3 = k_{3(H_2O)}/k_{3(D_2O)}$. The four simulated curves were generated with Z-RR-AMC and Z-FR-AMC: k_1 = 50 and 75 $\mu M^{-1} s^{-1}$, k_2 = 700 and 730 s^{-1}, k_3 = 70 and 400 s^{-1}, k_4 = 300 and

400 s^{-1}, k_5 = 800 and 1100 s^{-1}, k_7 = 6000 s^{-1}, k_9 = 8000 s^{-1}, k_{11} = 280 and 300 s^{-1}, k_{12} = 430 and 700 s^{-1}, k_{13} = 27 and 60 s^{-1}, k_{15} = 1500 s^{-1}, $^{D}k_1$ = 1.1, $^{D}k_3$ = 1.4, $^{D}k_7$ = 1.2 and 1.4, $^{D}k_{11}$ = 1.2 and 1.6, and $^{D}k_{13}$ = 1.4 and 1.9.

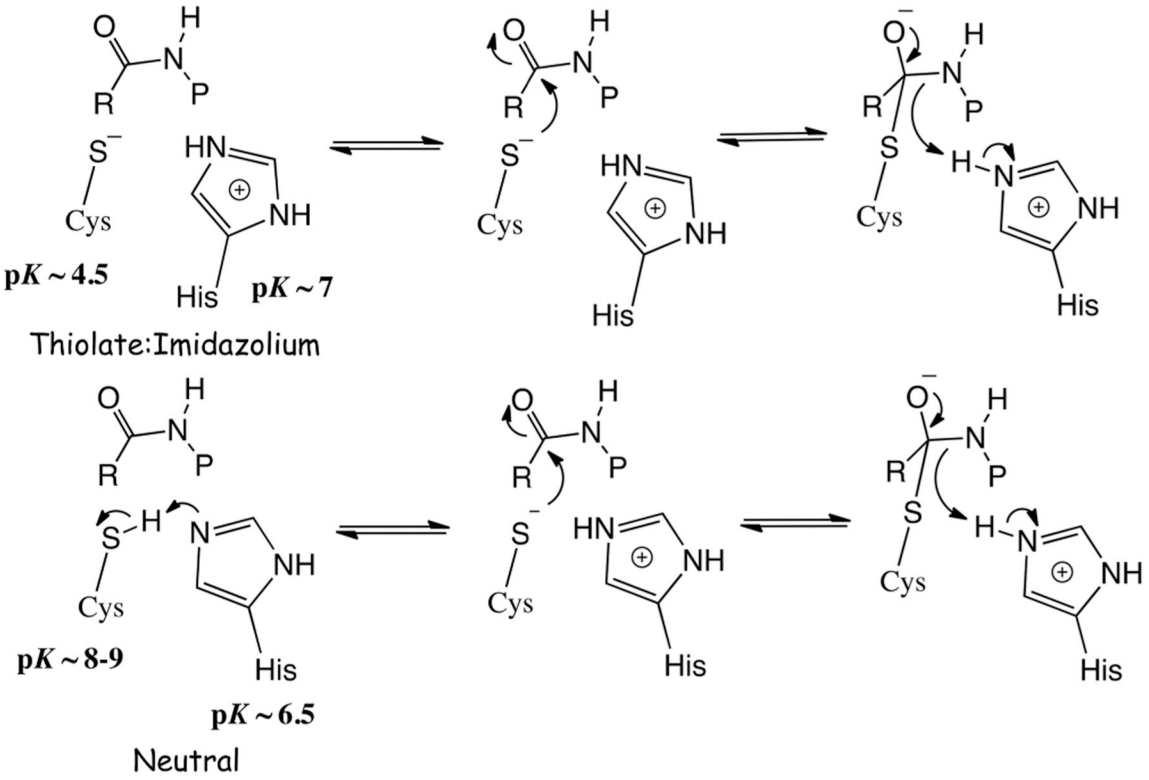

Scheme 1.

Potential Chemical Mechanisms for Cruzain of Attack of Thiolate on a Peptide Substrate Involving a Thiolate-Imidazolium or Neutral Cysteine-Histidine Dyad

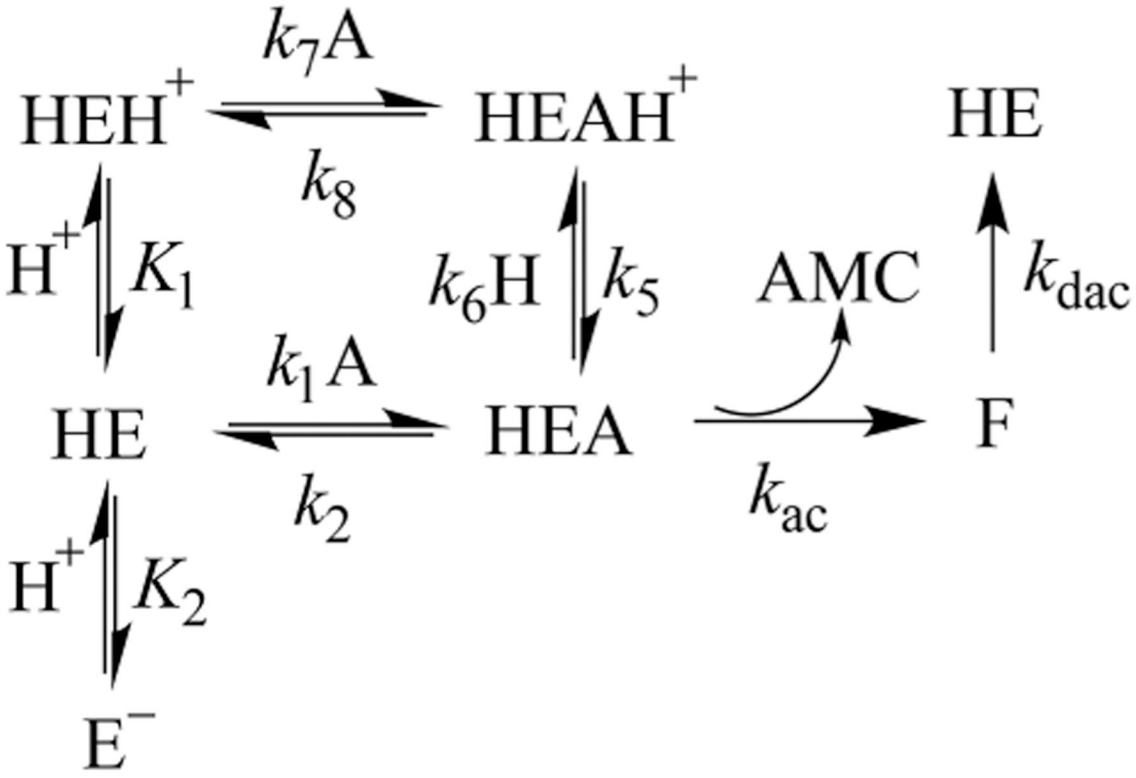

Scheme 2.
Kinetic Model for pH−Rate Profiles for Cruzain

Table 1.

Steady-state Kinetic Parameters for Cruzain-catalyzed Proteolytic Reactions of Z-FR-AMC, Z-RR-AMC and Z-RA-AMC.[a]

	Wildtype[b]			E208A[c]		
Substrate	$k_{cat}\left(s^{-1}\right)$	$K_m(\mu M)$	$k_{cat}/K_m\left(M^{-1}s^{-1}\right)$	$k_{cat}\left(s^{-1}\right)$	$K_m(\mu M)$	$k_{cat}/K_m\left(M^{-1}s^{-1}\right)$
Z-FR-AMC	17 ± 2	0.62 ± 0.02	$(2.7 \pm 0.4) \times 10^7$	21 ± 1	1.6 ± 0.1	$(1.3 \pm 0.1) \times 10^7$
Z-RR-AMC	7.2 ± 0.1	3.7 ± 0.4	$(1.9 \pm 0.2) \times 10^6$	0.27 ± 0.01	45 ± 4	$(6.0 \pm 0.1) \times 10^3$
Z-RA-AMC	0.89 ± 0.06	38 ± 2	$(2.3 \pm 0.3) \times 10^4$	0.017 ± 0.001	163 ± 3	$(1.0 \pm 0.1) \times 10^2$

[a]Under assay conditions of 50 mM MES, 50 mM TAPSO, 100 mM DEA, 1 mM CHAPS, 1 mM EDTA, 5 mM DTT, 2% (v/v) DMSO, pH 7.5 and 25 °C.

[b]The errors for wildtype-catalyzed reactions were determined from the average of kinetic parameters determined in duplicates.

[c]The errors for E208A cruzain mutant-catalyzed reactions are the standard deviations determined from the nonlinear least squares fits of the kinetic data.

Table 2.

pH-rate Profiles and Solvent Kinetic Isotope Effects from Steady-state Kinetics of Wild-Type Cruzain.[a]

		k_{cat}				k_{cat}/K_m						sKIE [b]	
Substrate	**Solvent**	**Eq.**	pK_1	pK_2 [c]	$c\left(s^{-1}\right)$	**Eq.**	pK_1	pK_2	pK_a	$c\left(\mu M^{-1} s^{-1}\right)$	β	$D_2O k_{cat}$	$D_2O\left(\frac{k_{cat}}{K_m}\right)$
Z-FR-AMC	H_2O	n.a. [e]	n.d. [d]	n.d.	14.5 ± 0.4	4	6.4 ± 0.7	n.d.	n.d.	24 ± 2		1.88 ± 0.06	1.4 ± 0.1
						5	6.2 ± 0.4	n.d.	5.8 ± 0.4	26 ± 2	70 ± 50		
	D_2O	n.a.	n.d.	n.d.	7.7 ± 0.1	4	6.0 ± 0.1	n.d.	n.d.	17 ± 1			
						5	6.0 ± 0.1	n.d.	5.2 ± 0.2	17.4 ± 0.7	34 ± 8		
Z-RR-AMC	H_2O	4	5.5 ± 0.1	≥ 10	7.4 ± 0.2	4	6.6 ± 0.1	9.6 ± 0.1	n.a.	0.23 ± 0.01	n.a.	1.76 ± 0.06	1.15 ± 0.08
	D_2O	4	5.9 ± 0.1	≥ 10	4.2 ± 0.1	4	7.4 ± 0.1	~ 10	n.a.	0.2 ± 0.01	n.a.		
Z-RA-AMC	H_2O	4	6.1 ± 0.1	≥ 10	0.88 ± 0.03	4	6.2 ± 0.1	≥ 10	n.a.	0.024 ± 0.001	n.a.	1.73 ± 0.07	1.09 ± 0.07
	D_2O	4	6.4 ± 0.1	≥ 10	0.51 ± 0.01	4	6.7 ± 0.1	≥ 10	n.a.	0.022 ± 0.001	n.a.		

Table 3.

Pre-Steady-State Kinetic Parameters of Cruzain-Catalyzed Hydrolysis of Z-FR-AMC and Z-RR-AMC in H_2O and D_2O[a]

substrate	solvent	$k_{cat}(s^{-1})$ [b]	$k_{ac}(s^{-1})$	$k_{dac}(s^{-1})$	$K_a(\mu M)$	$K_{ia}(\mu M)$ [c]
Z-FR-AMC	H_2O	30.5 ± 0.1	239 ± 6	35 ± 1	2.3 ± 0.1	9.8 ± 0.6
	D_2O	14.7 ± 0.1	179 ± 2	16 ± 1	0.86 ± 0.01	9.0 ± 0.7
	sKIE[d]	$D_2Ok_{cat} = 2.07 \pm 0.02$	$D_2Ok_{ac} = 1.34 \pm 0.01$	$D_2Ok_{dac} = 2.2 \pm 0.2$	$D_2OK_a = 2.7 \pm 0.1$	$D_2OK_{ia} = 1.09 \pm 0.11$
Z-RR-AMC	H_2O	15.2 ± 0.1	64.5 ± 0.2	19.9 ± 0.1	7.0 ± 0.1	14.0 ± 3.0
	D_2O	9.5 ± 0.1	46.1 ± 0.1	11.9 ± 0.1	5.5 ± 0.1	15.0 ± 3.0
	sKIE[d]	$D_2Ok_{cat} = 1.61 \pm 0.02$	$D_2Ok_{ac} = 1.40 \pm 0.01$	$D_2Ok_{dac} = 1.67 \pm 0.02$	$D_2OK_a = 1.27 \pm 0.03$	$D_2OK_{ia} = 0.93 \pm 0.27$

[a] Data were obtained as described in Experimental Procedures at pH(D) 7.5 in 10% (v/v) DMSO. The kinetic parameters were determined from global fitting according to eq 11.

[b] k_{cat} was calculated from k_{ac} and k_{dac}, and values of K_{ia} in H_2O and D_2O for both substrates were determined separately as described. The errors for all the kinetic parameters are the standard deviations determined from the nonlinear least-squares fitting of the data.

[c] Determined from fitting the transient burst rate vs substrate concentration according to eq 11.

[d] Solvent kinetic isotope effects as determined from the ratio of the two sets of kinetic parameters in H_2O and D_2O. The errors were calculated on the basis of the propagation of fractional errors.

Biochemistry. Author manuscript; available in PMC 2023 October 12.

Table 4.

Experimental and Calculated Kinetic Parameters for the Catalytic Mechanism of Cruzain.[a]

Substrate	Cbz-Arg-Arg-AMC			Cbz-Phe-Arg-AMC		
Kinetic Parameter	**Experimental Value**	**Calculated Value**	**Candidate Value**	**Experimental Value**	**Calculated Value**	**Candidate Value**
k_{cat}/K_a	$1.9 \pm 0.2\ \mu M^{-1} s^{-1}$	$4\ \mu M^{-1} s^{-1}$	$Dk_1 = 1.1$	$27 \pm 4\ \mu M^{-1} s^{-1}$	$25\ \mu M^{-1} s^{-1}$	$Dk_1 = 1.1$
K_{ia}	$14 \pm 3\ \mu M$	$14\ \mu M$	Dk_3 or $Dk_5 = 1.4$	$9.8 \pm 0.6\ \mu M$	$9.8\ \mu M$	Dk_3 or $Dk_5 = 1.4$
$D2O(k_{cat}/K_a)$	1.15 ± 0.08	1.14	$Dk_7 = 1.2$	1.4 ± 0.1	1.4	$Dk_7 = 1.3$
k_{ac}	64.5± 0.2 s^{-1}	65 s^{-1}	$Dk_{11} = 1.2$	239 ± 6 s^{-1}	239 s^{-1}	$Dk_{11} = 1.6$
$D2Ok_{ac}$	1.41 ± 0.01	1.2	$Dk_{13} = 1.4$	1.34 ± 0.01	1.2	$Dk_{13} = 1.9$
k_{dac}	19.9 ± 0.1 s^{-1}	20 s^{-1}	$a = k_3/k_2 = 0.14$	35 ± 1 s^{-1}	35 s^{-1}	$a = k_3/k_2 = 0.5$
$D2Ok_{dac}$	1.67± 0.02	1.6	$b = k_5/k_4 = 2.6$	2.2 ± 0.02	2.3	$b = k_5/k_4 = 5.0$
k_{cat}	15.2 ± 0.1 s^{-1}	15 s^{-1}	$c = k_6/k_7 = 0$	30 ± 1 s^{-1}	30 s^{-1}	$c = k_6/k_7 = 0.0002$
$D2Ok_{cat}$	1.61 ± 0.02	1.5	$d = k_5/k_7 = 0.13$	2.07 ± 0.02	2.08	$d = k_5/k_7 = 0.18$
K_a	$7.0 \pm 0.1\ \mu M$	4	$e = k_7/k_9 = 0.8$	$2.3 \pm 0.1\ \mu M$	1.2	$e = k_7/k_9 = 0.8$
$tKIE^{\circ}$	1.6	1.8	$x = k_{13}/k_{12} = 0.18$	2.2	2.1	$x = k_{13}/k_{12} = 0.1$
S_r	4	4	$y = k_{13}/k_{15} = 0.02$	70 ± 50	9	$y = k_{13}/k_{15} = 0.015$
			$k_1 = 50\ \mu M^{-1} s^{-1}$			$k_1 = 75\ \mu M^{-1} s^{-1}$
			$k_2 = 700\,s^{-1}$			$k_2 = 735\,s^{-1}$
			$k_3 = 100\,s^{-1}$			$k_3 = 400\,s^{-1}$
			$k_4 = 300\,s^{-1}$			$k_4 = 220\,s^{-1}$
			$k_5 = 800\,s^{-1}$			$k_5 = 1100\,s^{-1}$
			$k_6 = 0\,s^{-1}$			$k_6 = 1\,s^{-1}$
			$k_7 = 6000\,s^{-1}$			$k_7 = 6000\,s^{-1}$
			$k_9 = 8000\,s^{-1}$			$k_9 = 8000\,s^{-1}$
			$k_{11} = 280\,s^{-1}$			$k_{11} = 300\,s^{-1}$

Substrate	Cbz-Arg-Arg-AMC			Cbz-Phe-Arg-AMC		
Kinetic Parameter	Experimental Value	Calculated Value	Candidate Value	Experimental Value	Calculated Value	Candidate Value
			$k_{12} = 430\,s^{-1}$			$k_{12} = 700\,s^{-1}$
			$k_{13} = 55\,s^{-1}$			$k_{13} = 135\,s^{-1}$
			$k_{15} = 5000\,s^{-1}$			$k_{15} = 5000\,s^{-1}$

[a]Experimental kinetic parameters are those reported in Tables 2 and 3. Solvent equilibrium isotope effects, $(^{D}K_{eq} = 0.6 - 0.7$, and $^{D}K_{eq11} = 1.3)$, intrinsic isotope effects on each step $(^{D}k_{1-15})$, and microscopic rate constants (k_{1-15}) were obtained by dynamic simulation of the experimental pre-steady-state kinetic data using Kintek Explorer.[47] Candidate values obtained from these fittings were then inserted into eqs 14–21 to produce the calculated values in the table. Values for k_3 and k_{13} presented here resulted from extrapolation to an infinite concentration of the variable substrates to produce limiting values $k_{cat,}$ $k_{ac,}$ and k_{dac}.